Forschungszentrum Karlsruhe

Technik und Umwelt

Wissenschaftliche Berichte

FZKA 6597

Review and comparative assessment
of helium-cooled divertor concepts

S. Hermsmeyer, K. Kleefeldt

Institut für Kern- und Energietechnik
Programm Kernfusion

Final Report on EFDA Task TRP4

Review and comparative assessment
of helium-cooled divertor concepts

Abstract

Within the European Power Plant Conceptual Study (PPCS) started in 2000 it is planned to integrate a Helium cooled blanket with a divertor using the same coolant. The present work is intended to focus research on concepts that are capable of withstanding the large heat fluxes expected for the divertor.

Five divertor plate concepts – two from the first phase of the PPCS, one variation, and two concepts from the literature – are assessed on the basis of consistent assumptions and operating parameter ranges. While thermohydraulic performance is judged by maximum wall temperatures and pressure drop, thermal stresses are estimated based on temperature differences across the cooling channel.

The results show that thermal stress is the limiting quantity for all concepts. They confirm that (i) a large heat transfer coefficient on the fluid side; (ii) the delivery of low temperature coolant to the First Wall, i.e. a flow path transversal to the First Wall; and, (iii) the use of refractory metals are key elements of a Helium cooled divertor.

Vergleich heliumgekühlter Divertorkonzepte

Zusammenfassung

Im Rahmen der im Jahr 2000 begonnenen Europäischen Leistungsreaktorstudie ist die Integration eines heliumgekühlten Blankets mit einem ebenfalls heliumgekühlten Divertor geplant. Dazu gibt es einen Reihe von potentiellen Divertorkonzepten. Die vorliegende Arbeit soll Entwicklungen im Rahmen der Studie auf diejenigen Konzepte fokussieren, die das größte Potential für die Abführung der im Divertor anfallenden großen Wärmeströme besitzen.

Fünf Konzepte für den Aufbau von Divertorplatten – zwei aus der ersten Phase der Reaktorstudie, eine Variation dazu, sowie zwei Konzepte aus der Literatur – werden auf der Basis konsistenter Annahmen und Betriebsbedingungen bewertet. Dabei wird die thermohydraulische Leistungsfähigkeit nach maximaler Wandtemperatur und Druckverlust bewertet, während thermische Spannungen auf der Basis von Temperaturunterschieden an Vorder- und Rückseite des Kühlkanales überschlagen werden.

Die Ergebnisse bestätigen, daß (1) ein großer Wärmeübergangskoeffizient auf der Fluidseite, (2) der Zugang von kaltem Helium an allen Punkten der Ersten Wand, und damit ein Kühlmittelfluß senkrecht zur Ersten Wand, und (3) der Einsatz von Refraktormetallen zentrale Elemente eines heliumgekühlten Divertors sind.

Table of Contents

LIST OF TABLES

LIST OF FIGURES

1 Introduction

Within the European Power Plant Conceptual Study (PPCS) started in 2000 it is planned to integrate a Helium cooled blanket with an equally Helium cooled divertor, the reason being that (i) water as a coolant has to be avoided for safety reasons; and, (ii) Helium can be operated at much higher temperatures than water and will thus allow the roughly 10% of plant power reaching the divertor to raise the plants' efficiency significantly.

Helium-cooled divertor concepts studied in the preparatory phase to the PPCS and elsewhere promise to allow peak heat fluxes at the target plates up to the order of 5 to 6 MW/m^2 (which is close to the limits achievable with other coolant fluids). In order to improve the heat transfer at the solid/gas interface, the concepts employ different enhancement methods, like multi-channel flow, porous media, and micro-channels, each having specific pro's and con's with view to reactor application.

The present study was initiated with the aim of improving the understanding of the relative merit of the host of competing designs, and identifying the features that are mandatory for reaching the highest possible heat fluxes. Potential variants are reviewed and evaluated by means of limited thermohydraulic and thermomechanical analyses, based on a consistent set of basic assumptions and operating parameter ranges.

The different concepts of divertor target plates studied in this report are characterised in Chapter 2. Two other promising concepts are introduced briefly. They were not included in the detailed study because they would have required non-standard thermohydraulic analyses that could not be carried out in the short time available.

Chapter 3 contains the analyses carried out for the concepts, starting with a description of parameter ranges and of correlations used and moving to the presentation of thermohydraulic and thermomechanical results.

Chapter 4 summarises what have been found to be key elements for a high performance divertor design. Chapter 5 gives conclusions.

2 Review of helium-cooled divertor concepts

The divertor target plates in a fusion power reactor are rather large components. They are envisaged to be slightly bent structures, following the contour of the cross section of the divertor cassette, about 1.5 m x 1 m in size. These plates are assumed to consist of arrays of separate channels, with minimal gaps in between, running in poloidal direction. Groups of channels (or all channels of a plate) are connected to manifolds to provide inlet and outlet ports for the helium coolant. Free thermal expansion must be allowed in longitudinal (poloidal) direction relative to the supporting backbone, but only small out-of-plane deflections can be tolerated.

Many concepts of heat transfer enhancement in gas-cooled systems are found in the literature as has been reviewed in [1], but only a few are applicable to divertors, characterised by very high heat loads, large heated surfaces, effective heat conversion capability and stringent material requirements. Five concepts are of interest to be reviewed and compared in this sense:

i. Porous medium concept with a cross flow pattern (relative to the channel axis),

ii. Multi-channel concept with a bi-directional longitudinal flow scheme,

iii. Swirl rod concept using a helical wire in an annular channel as heat transfer enhancement,

iv. Eccentric swirl promoter concept, similar to (iii) but with multiple fins and eccentric core,

v. Slot concept, a derivative of (i) but replacing the porous medium by a narrow gap.

The first and second concept have been studied by two different groups (references [1] and [2]) in the frame of the European Programme "Preparation of a Power Plant Conceptual Study, Plant Availability" and was to exploit the limits of helium cooling of divertors with the special features of

producing high-grade heat. The third concept has been proposed by Baxi [3], also aiming at finding a compromise between efficient heat transfer and reasonable pressure drop. The fourth concept, eccentric swirl promoter [4], was originally designed for water cooling with the aim to raise the critical heat flux in the heavily loaded region of a coolant channel, but it seems attractive to also be used in gas-cooled systems. Finally, the slot concept, not investigated so far, is an attractive variant of the porous medium concept (i). It avoids the fabrication and bonding issues by substituting the porous body by a narrow gap, which approaches micro-channel dimensions.

The studies mentioned above started from different fundamental assumptions in terms of geometric requirements, thermal-hydraulics parameters, materials constraints, and methodologies and are thus not readily comparable in their concepts' performance. Therefore, the concepts are briefly introduced in the following sub-sections in their original appeal as stated by the respective authors. A comparison based on a set of consistent assumptions will then be made in section 3 beginning on page 11.

2.1 Porous medium concept

The porous medium divertor concept has been extensively studied in [1]. A typical cross section of the proposed channel structure is depicted in Figure 1 and the design characteristics are compiled in Table 1 on page 6. Main features are the porous layer for heat transfer enhancement between the coolant containing structure and the coolant itself, and the circumferential flow direction. The latter means that the coolant heats up within a given cross section according to the heat deposited locally, rather than integrated along the channel length. This is important for non-uniform heating profiles.

The variation of the cross section necessary to accommodate the tilted and bent shape of a divertor target plate was supposed to be small and has thus been ignored in the study. So the cross section of the divertor channel structure measures in that layout 36 mm x 39 mm and has a 28 mm diameter bore over the entire channel length.

The internals consist of the porous medium wick and two staggered and slit coolant tubes for helium inlet and outlet. Hence, the helium flow is forced from the inner tube via the upper slot into the wick, passes the wick in two halves and exits via the sickle-shaped duct between the two tubes. The wick insert is needed principally in the heavily loaded channel part only. The inlet tube should be tapered in order to balance flow velocities in longitudinal direction as schematically illustrated in Figure 2.

The insert and channel structure are assumed to be made from the same material, namely molybdenum or tungsten alloy to minimise differential thermal expansion. Firm bonding between the outer wick contour and the structure is essential for optimal thermal conduction, whereas the inner contact may be loose, perhaps even sliding at one channel end. The pressure conditions tend to open up the tubes at the upper slot and to squeeze the outlet tube at the back side. Therefore the opening shown at the rear side of the outlet tube may be a discontinuous slot or an array of holes.

A protection layer made of tungsten is attached to the channel structure, presumably by hot isostatic pressing (HIP). The thickness required is not known at present. If it is in the range of a few millimeters, chemical vapour deposition can also be considered as plating method. The armour is castellated in order to avoid extra thermal stresses. The channel shape in the back has little impact on the thermomechanical behaviour and has been arbitrarily assumed as flat.

The thermal-hydraulic parameters were driven by the requirement to meet the materials temperature windows (minimum coolant temperature at the target plate of 600 °C), to get attractive conditions for power conversion, to keep the pumping power low, and yet to obtain favourable heat transfer coefficients. The study in [1] led to the parameter choice listed in Table 1.

The following conclusions were drawn. Peak heat fluxes of 5.5 to 6 MW/m^2 are feasible with this concept, given that the operating temperature in the only structural materials deemed viable (molybdenum and tungsten alloys) must not fall below 600-700 °C for reasons of embrittlement. Heat flux limits are given by stress criteria, but also temperature limits and deflection constraints have to be observed. A 2-point support causing substantially lower stresses compared to a 3-point support would lead to excessive out-of-plane deflection. The potential for further improvements through better heat transfer, material characteristics and design optimisation are marginal. Coolant parameters can be kept

in an attractive range for power conversion, e.g., inlet/outlet temperature at the whole divertor cassette of 400 °C/800 °C at 8 MPa, allowing an extra electric output of between 6 and 9 % of fusion power.

2.2 Multi-channel concept

The multi-channel concept [2] presents the effort to keep straight cooling channels in the divertor while achieving acceptable thermal stresses by means of minimised temperature differences across the channel.

Two co-axial circular pipes with inner diameters of 30 and 34 mm, respectively, build a double containment that withstands the coolant pressure with some margin. From a thermal and structural view this double pipe is proposed to be regarded as one element only. A channel insert divides the internal pipe into a plasma-facing cold leg consisting of four sub-channels, and a rear-side hot leg. On leaving the cold leg the coolant enters a 180 degree collector bend that guides it back into the hot leg. Large helium velocities in the cold leg raise the heat transfer and the coolant capability on the plasma-facing side of the pipe. Of the four sub-channels, fed in parallel, the two lateral ones are larger with the effect that heat transfer coefficients there are even higher than in the central channels, the idea being that this will broaden the plasma-facing zone of high heat flux.

The hot leg in the back has a relatively large hydraulic section to minimise local pressure drops, since it is unnecessary to stride for high heat transfer coefficients in this zone. The hot leg coolant and its neighbouring divertor structure is (are) roughly at the same temperature.

Although the concept is tailored to minimise temperature gradients at the location of the most critical temperatures and stresses near the half-way turn, calculations of thermal stress have led to the proposal of limiting the length of the divertor channel to 0.5 m. The concept is proposed to operate at 14 MPa helium pressure and a helium temperature increase of 51 K .

Comments:

While the choice of concept parameters in [2], in particular the limit on divertor length was noted, the comparison of concepts was nevertheless carried out using the parameter set justified in Section 3.1.1; alternative concepts would draw equal benefit from less stringent requirements.

The authors of the present report have attempted to re-evaluate the thermal-hydraulic performance by means of standard thermo-hydraulic correlations and by the use of a 3D finite element model. The comparison with results from [2] shows that heat transfer coefficients here are larger by about 20%, which is within an expected margin. However, the pressure loss of 0.63 MPa is in stark contrast with values of about 0.08 MPa quoted in [2]. As to structural temperatures, there is an equally gross difference between the up to 1270 ºC, depending on the wall contact of the flow channel insert, from the present f.e. model and the value of 968 ºC quoted in [2]. These differences imply that the concept will appear less favourable from comparisons below than anticipated elsewhere.

The models used and values from the benchmark are given in sections 3.1.2.3 and 3.1.3.2.

2.3 Swirl rod insert concept with 2D roughness

The swirl rod insert proposed by Baxi and Wong [3] is shown schematically in Figure 4 and the design parameters are given in Table 3 as far as they have been reported in the reference. It consists of a tube 11 mm in diameter, 1.5 mm wall thickness and a concentric solid insert of 6 mm, both forming an annular flow channel. Spacing is achieved by a helical wire, which produces a swirl flow in the annulus. The heat transfer between the outer shell and the coolant is enhanced by means of longitudinal grooves, approximately 0.1 mm deep. These grooves are foreseen at locations of high heat load only, i.e., on about 50 % of the perimeter and 50 % of the channel length, depending on the heat flux profile.

The helium inlet temperature is given as 200 °C with tungsten as reference structural material (alternatively vanadium or copper alloy). Typically, an effective heat transfer coefficient of 11000 to 22000 $W/(m^2K)$ is required to limit the surface temperature to 800 °C. At a system pressure of 4 MPa a pressure drop of 0.005 to 0.025 MPa per meter channel length has been evaluated. It is claimed that

the configuration can take peak heat fluxes as high as 5 to 10 MW/m^2, when the average heat flux across the heated length of 1 m is of the order of 1 MW/m^2. Few remarks concerning heat flux limits and allowable temperatures are given at the bottom of Table 3.

Comments:

The authors of the present report have attempted to re-evaluate the thermal-hydraulic performance for the case 4 studied in [3] with W as heat sink material and a peak heat flux of 10 MW/m^2. The results quoted could not be verified. In particular, the temperature rise of 32 K leads to excessive velocity and pressure drop.

2.4 Eccentric swirl promoter concept

The eccentric swirl promoter (ESP) is a means to enhance coolant flow conditions in high heat flux components, in which the heat is essentially applied from one side. Therefore, the ESP consists of a non-axisymmetric insert with helical fins, forming parallel coolant sub-channels, which vary periodically in size along their spiral length. Hence, high velocities and enhanced heat transfer are obtained at the heated side of the assembly, and lower velocities with reduced pressure drop prevail at the rear side. The sub-channels have nearly identical flow resistance as long as the total channel length is a multiple of the fin twist pitch.

The swirl-type flow pattern tends to reduce the overall temperature gradients within cross sections of the assembly, although not as effectively as other concepts do, because the partly heated coolant stream arrives at the back of the assembly only after travelling half way around the helix, i.e., typically 100 mm downstream. This is no big effect for uniform heat flux profiles but it is considerable for strongly peaked profiles.

A computer program has been set up to describe the channel geometry with its various parameters, the simplified heat transport from the assembly surface to the inner surface of the main tube, and the thermal-hydraulics in the individual sub-channels. The latter include the pressure losses, flow distribution, and the wall/coolant heat transfer coefficient for smooth or rough walls. The system is flexible in terms of size, number of fins, eccentricity etc. A parameter study revealed that a reasonable configuration is the one shown in Figure 6 on page 29, i.e., with 12 fins and an eccentricity of 2 mm for an assumed subassembly width of 36 mm. The thermal-hydraulic performance can be seen from Table 4 as an example. This example was chosen to resemble the conditions of the porous medium reference concept in its outer dimensions. At a helium velocity of about 250 m/s quite attractive heat transfer coefficients of 21000 W/(m^{2}K) can be achieved in the front region. The pressure drop of 0.42 MPa in a 1.2 m long assembly is tolerable. It is interesting to note that with this geometry the sub-channel cross section varies along its length by a factor of 3.4 (max/min). Further cases will be discussed in section 3 in the direct comparison of all concepts.

2.5 Slot concept

This concept has been derived from the porous medium concept by replacing the porous layer by a narrow gap. It has the advantage of avoiding the potential bonding problems between the outer structure and the porous layer and eases fabrication. On the other hand, the gap must be very small, ranging between 0.1 and 0.2 mm. The minimum gap is assured by means of small ribs, approximately 5 mm apart in longitudinal direction.

The inlet duct is tapered in order to optimise the pressure drop and to influence the longitudinal flow distribution both in the slot and in the duct. For a uniform heat flux, the slot flow distribution should also be uniform. There are several ways of shaping the inlet duct. One way would be to make it a cone, i.e., a linear reduction of the inner diameter between both ends. In that case the flow cross section in the duct would decrease in longitudinal direction faster than the mass flow rate would decay, leading to uneven axial velocity distribution. An alternative is to reduce the flow area linearly in accordance with the flow rate, which results in a more complicated shape of the duct. Both methods have been studied and the impact on the axial flow distribution in the slot was found to be small.

4

The small gap makes the system sensitive to differential thermal expansion and, therefore, to a redistribution of flow rate over the channel length. For instance, when using a thermal expansion coefficient of the structure and duct material of 6×10^{-6} K^{-1} and an average temperature difference between both parts of 150 K, the gap would grow by 25 microns, that is 12 to 25 % of the original gap width. The effect needs further attention, particularly for non-uniform heat load profiles. The results of thermal-hydraulic analysis are reported in section 3.1.3.5.

2.6 *Other concepts studied in the literature*

While it has been tried to cover promising divertor concepts, two alternative schemes will be described below that are deemed promising yet could not be studied within the resources of this task. The main reasons for their omission are: (i) their coolant channels are such that standard correlations for pressure loss and heat transfer do not apply, with no resources available to do further research; (ii) the concepts have been drawn up and tested for small specimens, but it is unclear how they would be realised on the scale of a fusion divertor geometry. Thus, design integration as a prerequisite for a serious concept study is lacking; and (iii), manifolding of these concepts is unclear, yet it is as critical as heat transport from the First Wall.

The following concepts are subject to continuing research and might play a role in future divertors.

2.6.1 Porous metal Tungsten heat exchanger

The unit cell of this concept [9] is a Tungsten cylinder perpendicular to the First Wall, with the First Wall end cap containing a hemispherical shell of brazed Tungsten porous metal. Helium coolant is blown into the cylinder and removed through a central pipe connected to the centre of the porous metal insert.
Experiments were carried out for an assembly of two cylinders of 32 mm diameter and 77 mm length cooled in parallel. Coolant Helium was at 4 MPa pressure and about 50 °C. The heat load was applied by means of an electron beam.
It is put down to different insert porosities in the two cylinders that mass flows and thus cooling conditions were quite different in the two cylinders. Measured uniform heat loads for the two cylinders were 5.9 and 5.5 MW/m^2, respectively, with pressure drops up to 55 kPa.

2.6.2 Hexagonal array micro-channels heat exchanger

This concept [10] again features a coolant flow perpendicular to the First Wall. Its manufacturing method is taken from micro systems technology, with four functional layers being machined and then joined together. The layers are, starting from the back: (1) the inlet manifold; (2) the outlet manifold layer that contains passages for inlet Helium; (3) the micro-channel layer that is the main body of the divertor, with a hexagonal arrangement of hexagonal inlet channels and rectangular outlet channels; and (4), the facesheet that holds grooves for a 180 degree turn of the coolant from the inlet into the outlet channels. The facesheet is the key cooling structure with the Helium directional change producing high heat transfer coefficients on its back side and the large divertor heat loads entering at its front.

Table 1: Porous medium concept design characteristics

Design features: [1]	
- Porous medium heat transfer enhancement - Circumferential split flow - Axially tapered inlet flow channel - Single-wall structure	
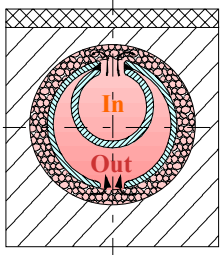
Geometrical parameters:	
Unit cell width (toroidally), mm	36
Channel diameter, mm	28
Porous layer thickness, mm	3
Porous medium void fraction, %	40
Channel length, mm	1600
Heated length (porous medium insert length), mm	1000
Minimum thickness of structure at heated side, mm	3
Reference armour thickness, mm	3

Thermal hydraulics:	
Coolant temperature at target plate in/out, °C	632/800
Coolant temperature at divertor cassette in/out, °C	400/800
Coolant system pressure, MPa	8
Mass flow rate	
Maximum flow velocity, m/s	140
Typical effective heat transfer coefficient, $W/(m^2 K)$	20000
Pressure drop at target plate, MPa	0.45
Pressure drop at divertor cassette, MPa	0.65

Materials:	
Structure (coolant containment), reference	Mo-alloy (TZM)
Structure (coolant containment), alternative	W-alloy
Armour, reference	W
Minimum operating temperature for structural material (guideline), °C	600-700
Allowable stress of structural material (3Sm value), MPa	360 (at 1100 °C)

Performance:	
Heat flux limit, MW/m^2	5.5
Average heat flux across heated length, MW/m^2	3
Toroidal linear power at target plates, MW/m	3
Nuclear volumetric heating power in target plate	neglected
Ratio of blower power to target plate thermal power	

Remarks: Stress analysis with 3D model and 3-point support of target plate; no credit taken of channel heating at the back side due to hot coolant stream; porous layer can be tailored to reduce pressure loss; quoted heat transfer coefficient is speculative.
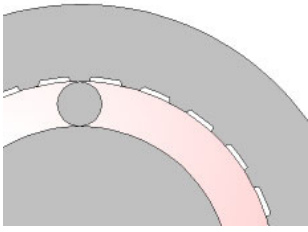
Table 2: Multi-channel concept design characteristics

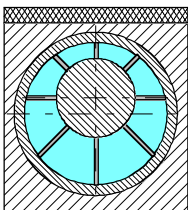| Design features: [2]	
- Bi-directional multi-channel flow - Reduced temperature gradients through hot outlet channel - Limited channel length - Double-wall pressure containment	
Geometrical parameters:	
Unit cell width (toroidally), mm	40
Channel diameter, mm	30
Porous layer thickness, mm	not applicable
Porous medium void fraction, %	not applicable
Channel length (two axial sections), mm	2 x 500
Heated length, mm	2 x 500
Minimum thickness of structure at heated side, mm	2 + 3
Reference armour thickness, mm	3
Thermal hydraulics:	
Coolant temperature at target plate in/out, °C	500/551[1]
Coolant temperature at divertor cassette in/out, °C	not considered
Coolant system pressure, MPa	14
Mass flow rate	0.34 – 0.4
Maximum flow velocity, m/s	*280*
Typical effective heat transfer coefficient, W/(m^{2}K)	15000 – 20000
Pressure drop at target plate, MPa	0.15[2]
Pressure drop at divertor cassette, MPa	not considered
Materials:	
Structure (inner pressure tube), reference	W
Structure (outer channel casing), reference	W
Flow channel insert	*W*
Armour, reference	W
Minimum operating temperature for structural material (guideline), °C	550 – 600
Allowable stress of structural material (3Sm value), MPa	786 at 710 °C, 750 at 755 °C, 722 at 790 °C
Performance:	
Heat flux limit, MW/m^2	5
Average heat flux across heated length, MW/m^2	*5*
Toroidal linear power at target plates, MW/m	*5*
Nuclear volumetric heating power in target plate, MW/m^3	20
Ratio of blower power to target plate thermal power	0.017
Remarks: Stress analysis assumed plane strain model; allowable stress for stress relieved condition in not conservative; turbulence promoters considered as potential heat transfer enhancement means.	

---

[1] Outlet temperature ranges from 551 to 567 °C depending on mass flow rate of 0.4 to 0.3 kg/s, respectively.
[2] Refers to inlet channels including the flow reverse chamber

Table 3: Swirl rod insert characteristics

Design features: [3] - Swirl rod insert with helical wire or rib - 2D roughness (longitudinal grooves) at tube inner wall - Grooves on 50 % of length and 50 % of perimeter - Single-wall structure	
Geometrical parameters: Unit cell width (toroidally), mm Channel diameter, mm Groove dimensions, depth x width (typical), mm Helical wire height and pitch of helix respectively, mm Channel length, mm Heated length, mm Minimum thickness of structure at heated side, mm Reference armour thickness, mm	11 8 0.1 x 0.7 1 and 250 1000 1000 1.4 not considered
Thermal hydraulics: Coolant temperature at target plate in/out, °C Coolant temperature at divertor cassette in/out, °C Coolant system pressure, MPa Mass flow rate, kg/s Maximum flow velocity, m/s Typical effective heat transfer coefficient, W/(m^{2}K) Pressure drop at target plate, MPa Pressure drop at divertor cassette, MPa	200/232 – 280 not considered 4 not reported not reported 11000 - 22400 0.005 – 0.025 not considered
Materials: Structure (coolant containment), reference Structure (coolant containment), alternative Armour, reference Minimum operating temperature for structural material (guideline), °C Allowable stress of structural material (3Sm value), MPa	W V and Cu not considered 20 not considered
Performance: Heat flux limit, MW/m^2 Average heat flux across heated length, MW/m^2 Toroidal linear power at target plates, MW/m Nuclear volumetric heating power in target plate Ratio of blower power to target plate thermal power, %	5 - 10 1 1 neglected 0.25 – 3.2
Remarks: No stress analysis results have been reported; heat flux limit is solely evaluated from maximum temperature at tube surface; maximum temperature at tube surface is assumed as 800 °C for W and V, and 500 °C for Cu; minimum allowable structural temperature for W and V has not been discussed.	

Table 4: Eccentric swirl promoter characteristics

Design features: [4] - Eccentric core insert with helical ribs - Channel size and, hence, velocity change periodically - Good heat transfer coefficient where needed - Reduced pressure drop elsewhere - Channel tube is optional	
Geometrical parameters: Unit cell width (toroidally), mm Channel tube inner diameter, mm Eccentric core diameters (typical), mm Offset of core from main channel centre (eccentricity), mm Number of fins and fin twist pitch for a 2π angle, mm Channel length, mm Heated length, mm Minimum thickness of structure at heated side, mm Reference armour thickness, mm	 36 28 20 2 12 and 200 1200 1000 3 3
Thermal hydraulics: Coolant temperature at channels forming the target plate, in/out, °C Coolant temperature at divertor cassette in/out, °C Coolant system pressure, MPa Mass flow rate, kg/s Maximum flow velocity, m/s Typical effective heat transfer coefficient, W/(m^{2}K) Pressure drop at target plate, MPa Pressure drop at divertor cassette, MPa	 600/800 400/800 14 0.173 250 21000 0.42 not considered
Materials: Structure (coolant containment), reference Structure (coolant containment), alternative Armour, reference Minimum operating temperature for structural material (guideline), °C Allowable stress of structural material (3Sm value), MPa	 Mo-alloy (TZM) W-alloy W 600-700 tbd
Performance: (see remarks below) Heat flux limit, MW/m^2 Average heat flux across heated length, MW/m^2 Toroidal linear power at target plates, MW/m Nuclear volumetric heating power in target plate Ratio of blower power to target plate thermal power, %	 4 – 5 5 5 neglected 5.4
Remarks: Stress analysis has not been performed. The heat flux limit is a guess based on results obtained in [1]. The thermal-hydraulic results pertain to a uniform heat load of 5 MW/m^2 across the heated length of 1 m and a total length of 1.2 m (see also section 3).	

Table 5: Slot concept design characteristics

Design features: - Narrow peripheral gap enhances heat transfer - Circumferential split flow - Axially tapered inlet flow channel - Single-wall or double-wall structure	
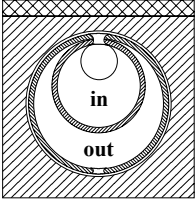
Geometrical parameters (compare Figure 7):	
Unit cell width (toroidally), w_M, mm	36
Channel diameter, $2R$, mm	28
Peripheral gap width, mm	0.15
Peripheral spacer ribs, axial width and pitch, respectively, mm	0.5 and 5
Channel length, mm	1200
Heated length, mm	1000
Minimum thickness of structure at heated side, mm	3
Reference armour thickness, mm	3

Thermal hydraulics:	
Coolant temperature at target plate in/out, °C	600/800
Coolant temperature at divertor cassette in/out, °C	not considered
Coolant system pressure, MPa	14
Mass flow rate, kg/s	0.17
Maximum flow velocity, m/s	75
Typical effective heat transfer coefficient, $W/(m^2K)$	14000
Pressure drop at target plate, MPa	0.14
Pressure drop at divertor cassette, MPa	not considered

Materials:	
Structure (coolant containment), reference	Mo-alloy (TZM)
Structure (coolant containment), alternative	W-alloy
Armour, reference	W
Minimum operating temperature for structural material (guideline), °C	600-700
Allowable stress of structural material (3Sm value), MPa	not considered

Performance:	
Heat flux limit, MW/m^2	4 – 5
Average heat flux across heated length, MW/m^2	5
Toroidal linear power at target plates, MW/m	5
Nuclear volumetric heating power in target plate	neglected
Ratio of blower power to target plate thermal power	0.017

Remarks: Stress analysis has not been performed. The heat flux limit is a guess based on results obtained in [1]. The thermal-hydraulic results pertain to a uniform heat load of 5 MW/m^2 across the heated length of 1 m and a total length of 1.2 m (see also section 3).

3 Comparative assessment of divertor concepts

The divertor concepts characterised in chapter 2 will be compared in the following, mainly in terms of their thermal-hydraulic performance. The mechanical aspects can only be addressed qualitatively within this task in section 3.2.

3.1 Thermal-hydraulic performance

In assessing the thermal-hydraulic performance of the different concepts we are mainly interested in comparing the pressure loss and the structural temperature distribution for given sets of coolant and load parameters. The pressure loss, in turn, is related to the pumping power needed to circulate the coolant through the flow channels. Therefore, the ratio of pumping power to thermal power removed is an interesting qualifier and will be emphasised. The temperature distribution in the structure is intimately correlated with the heat transfer coefficient achievable, but also with the coolant routing through the subassembly. Hence, the heat transfer coefficients will be evaluated. Finally the mass flow rate and the maximum velocity anywhere in the subassembly are observed. The latter is to prove that the incompressible flow modelling adopted is justified. The assessment will be made for a consistent set of parameters outlined in the next section and by use of essentially the same methods and tools described in section 3.1.2. The results will then be presented and discussed in sections 3.1.3 to 3.1.4.

3.1.1 Rationale to select parameter ranges

3.1.1.1 Coolant parameters

Main thermal-hydraulic parameters in divertor design are the coolant temperature level, the temperature rise in the divertor (more specifically in the target plate), and the system pressure. They are strongly dictated by material constraints. For instance, when choosing a copper alloy as structural material because of its excellent thermal conductivity, the maximum temperature in the structure is limited to about 450 °C, leading inevitably to a low temperature cooling system with in-attractive capability for heat conversion. Refractory alloys, on the other hand, call for relatively high operating temperatures with view to radiation embrittlement, setting a lower boundary for the coolant temperature. In this study emphasis is placed on refractory alloys as structure with a high temperature cooling system and the potential for good conversion efficiency.

The minimum allowable operating temperature for refractory alloys like tungsten or molybdenum-based is still a matter of debate. In accordance with the discussions in the frame of the PPA study [1] we chose 600 °C as the lower limit. Thus, the minimum coolant temperature at the entrance to the divertor target plate is assumed as $T_{Target,in}$=600 °C. On the other hand, the coolant temperature should not be chosen too high in order to cope with allowable stress limits in the divertor target plate as well as in the hot leg of the coolant circuit. An outlet temperature of $T_{Target,out}$=900 °C seems to be a reasonable upper boundary.

For the benefit of power conversion efficiency, e.g. in a closed loop Brayton cycle, the temperature rise in the whole divertor circuit should be chosen high. This reduces the mass flow rate in the circuits, leading to smaller piping. However a large temperature rise entails lower flow velocities in the target plates and thus impedes the heat transfer in the coolant channels. Therefore, the optimum temperature rise in the target plate, ΔT_{Target}, is a trade-off and may vary between different designs. In the recent divertor study [1] a temperature rise at the target plates of 168 K was found to be suitable for the porous media concept, in combination with another ΔT of 232 K occurring in the rest of the divertor components cooled in series with the target plates. Based on this scheme, a range of ΔT_{Target}=100 to 250 K at target plates and, consequently, $\Delta T_{Divertor}$=200 to 500 K for the whole divertor seem to be a reasonable approach for power reactor application.

The third important parameter in target plate layout is the system pressure, $p_{Divertor}$. Again, a trade-off has to be made between stress limits, pumping power, size of piping, and heat transfer coefficients in

coolant channels. A moderate system pressure of 8 MPa was proposed in [1] and up to 14 MPa in other studies like for instance in [2]. Therefore, the whole range of 8 to 14 MPa has been considered in the present study. It should be noted that this pressure in the divertor loop (primary circuit) has no direct influence on the choice of the pressure in the secondary circuit of the Brayton cycle, which may be substantially higher.

Note: A brief investigation has been performed to show the influence of key temperatures on the power conversion efficiency utilising a high pressure closed-loop Brayton cycle for extracting the heat from the divertor system via an intermediate heat exchanger [5]. For the divertor cooling cycle it was assumed as said before that the coolant is circulated in series at first through the bulk of the divertor structure and subsequently through the target plates. Half of the total divertor power be generated in the target plates and half of it is produced in the rest of the divertor. From this assessment we conclude: (i) Increasing the divertor outlet temperature gains cycle efficiency (about 5 points per 100 K). (ii) Reducing the divertor inlet temperature while keeping the outlet constant has little influence on the cycle efficiency. (iii) If the temperature rise in the whole divertor becomes less than 200 K, the efficiency goes down dramatically.

We conclude from this background to chose the reference values and ranges for the divertor cooling system parameters in this study as follows:

Table 6: Thermal-hydraulic parameters considered in this study

Parameter	Reference value	Range
Inlet temperature to target plate	600 °C	600 – 800 °C
Temperature rise at target plates	200 K	100 – 250 K
Temperature rise at whole divertor	400 K	200 – 500 K
System pressure (primary circuit)	8 MPa	8 – 14 MPa

3.1.1.2 Geometrical and load parameters

The study starts from the presumption that the divertor is of the single-null type, located at the bottom of the tokamak and similar to the ITER design. Thus the circular divertor arrangement is supposed to be made up of a number of segments (cassettes) each one consisting, besides other elements, of an inboard and outboard target plate as the heaviest loaded components of a tokamak. The expected size of a single outboard target plate (1 of 48) in a power reactor is about 1.2 m in toroidal and 1 to 1.5 m in poloidal direction. It is envisaged that each target plate is made up of an array of parallel assemblies running poloidally and being connected at the ends to coolant headers. The principal configuration of such an assembly is shown in Figure 8. The concepts discussed here differ mainly in their design of the flow inserts as sketched in Table 1 through Table 5.

From this overall picture of the target plate design and from the assumption that the plates are exposed to high heat loads over about 80 % of their length at maximum, the geometrical parameter ranges for thermal-hydraulic analysis have been defined for a single subassembly. The expected mean heat load at the target plates in a power reactor is of the order 3 MW/m^2 [1] if a rather flat load profile, spread over a poloidal width of 1 m, can be achieved. There is however large uncertainty in predicting either the total load, the load distribution and the inboard/outboard division, so that a range of 3 to 6 MW/m^2 has been assumed in this assessment. Below is a summary of geometrical and load parameters used (see also Figure 8).

- Total channel length (equipped with flow insert): 0.8 to 1.2 m

- Heated length: 0.6 to 1.0 m (with non-heated margin of 0.1 m at both ends)

- Average assembly width: 0.018 to 0.04 m (reference width is 0.036 m)

- Average surface heat load (on area defined by heated length by width): 3 to 6 MW/m^2

- Axial heat load profile: uniform (for stress considerations also peaked, see section 3.2.2).

12

Review and comparative assessment of Helium cooled divertor concepts

3.1.2 Method of analysis

For most of the concepts standard correlations for heat transfer and pressure drop in smooth or rough channels as documented in the VDI-Wärmeatlas [6] have been used. This applies to the MC, SRI, ESP and SLOT concept. Extra heat transfer enhancement methods as proposed for the SRI by specially machined roughness (2D of 3D) have deliberately not been considered, since they can be used in principle with any one concept in one or the other form. Only for the PM concept special equations have been applied. Below are reproduced the equations for plain channels (with smooth walls or natural roughness), followed by explanations on special implications pertaining to individual concepts.

3.1.2.1 General equations for plain channels

Heat transfer coefficient in plain channels with smooth or rough walls [6]:

(1)
$$h = \frac{k}{d_h} \cdot \frac{\frac{\xi}{8} \cdot (\text{Re} - 1000) \cdot \text{Pr}}{1 + 12.7\sqrt{\frac{\xi}{8}} \cdot \left(\text{Pr}^{0.67} - 1\right)} \cdot \left[1 + \left(\frac{d_h}{l}\right)^{0.67} \right] \cdot K^*$$

where

$$\xi = \left(1.82 \cdot \log_{10}(\text{Re}) - 1.64 \right)^{-2}$$

$$K^* = \left(T_{Fluid} / T_{Wall} \right)^{0.45}$$

valid for: $2300 \le \text{Re} \le 10^6$, $\quad 0.5 \le \text{Pr} \le 10^4$, $\qquad 0 \le d_h / l \le 1$ and with

h	[W/(m²K)]	Heat transfer coefficient
k	[W/(mK)]	Thermal conductivity of the fluid
d_h	[m]	Tube inner diameter
Re	[1]	Reynolds number
Pr	[1]	Prandtl's number
l	[m]	Length of channel
K^*	[1]	Factor to correct for wall temperature[3]
T	[K]	Temperature

Pressure drop in plain channels

The pressure change in a single-phase flow in a straight channel is usually written as

(2)
$$\frac{dp}{dz} = -f \cdot \frac{\rho_B \cdot v^2}{2 \cdot d_h}$$

where	f	=	friction factor
	ρ_B	=	bulk fluid density
	v	=	cross sectional average fluid velocity
	d_h	=	channel hydraulic diameter

Many empirical correlations exist for the friction factor, f. Unless otherwise stated, we have used the approximation proposed by Moody [8]. It includes the dependence from the relative wall roughness, R_t / d_h, and from the Reynolds number, Re, as follows:

---

[3] K^* has been set equal to 1 in this assessment.

$$f = 0.0055 \cdot \left\{ 1 + \left[2 \cdot 10^4 \cdot \left(\frac{R_t}{d_h} \right) + \frac{10^6}{\mathrm{Re}} \right]^{\frac{1}{3}} \right\}$$

and is valid in the following ranges when allowing deviation of ±5 %

$$\frac{R_t}{d_h} \le 0.01 \qquad\qquad f \le 0.05 \qquad\qquad 4 \cdot 10^3 \le \mathrm{Re} \le 10^7$$

where R_t is the average roughness height.

3.1.2.2 Equations and model used for the porous media concept

The equations developed by Rosenfeld [7] have been adopted to compute the heat transfer and pressure drop in the porous layer, although in a modified manner as will be explained. For the pressure drop in the inlet and outlet ducts equation (2) from section 3.1.2.1 was used.

Heat transfer coefficient

The effective heat transfer coefficient, understood as the inverse heat resistance between the solid channel wall and the bulk gas temperature caused by the porous medium, reads [7]

(4)
$$h_0 = \varepsilon \cdot h_p + \sqrt{h_p \cdot k_p \cdot S_p}$$

In this model the local particle-to-fluid heat transfer coefficient, h_p, is expressed in the form

(5)
$$h_p = 1.064 \cdot \bar{c}_p \cdot G \cdot \left(\frac{\bar{c}_p \cdot \mu_f}{k_f} \right)^{-2/3} \cdot \mathrm{Re}^{-0.41}$$

for $\mathrm{Re} \ge 350$, i.e., turbulent flow and

(6)
$$h_p = 18.1 \cdot \bar{c}_p \cdot G \cdot \left(\frac{\bar{c}_p \cdot \mu_f}{k_f} \right)^{-2/3} \cdot \mathrm{Re}^{-1}$$

for $\mathrm{Re} \le 40$, i.e., laminar flow.

Here the Reynolds number is defined by use of the superficial mass velocity and the particle diameter:

(7)
$$\mathrm{Re} = \frac{G \cdot D_p}{\mu_f}$$

ε		Porosity of the porous layer (wick)
k_p	W/(mK)	Thermal conductivity of wick material
S_p	m²/m³	Specific surface of wick
$\bar{c}_p$	Ws/(kg K)	Specific heat of fluid at mean temperature
G	kg/(m²s)	Superficial mass velocity in wick
μ_f	kg/(ms)	Dynamic viscosity of fluid
k_f	W/(mK)	Thermal conductivity of fluid
D_p	m	Particle diameter of wick

It was found in the earlier study [1], that equation (4) gives unrealistically high values for the heat transfer coefficient (up to 50000 W/(m²K)), which are not in agreement with results from small-scale

experiments reported in the literature. One reason for the discrepancy may be that the model was developed for a water-cooled test article made of copper, and may not be valid for a gas-cooled design made from refractory materials. When however equation (5), supposed to describe the local particle-to-fluid heat transfer, is taken as the effective heat transfer coefficient, values seem quite reasonable, namely of the order 20000 W/(m²K). This value was also accepted after long discussions as a realistic goal in porous media heat exchanger development. Therefore, in lieu of proven models, equation (5) instead of equation (4) was used to compute the effective heat transfer coefficient in the porous medium design, knowing that this is speculative.

Pressure drop in the porous layer

$$(8) \qquad \frac{\Delta p}{\Delta l} = \frac{G}{\rho_B \cdot D_p} \cdot \frac{(1-\varepsilon)}{\varepsilon^3} \cdot \left(\frac{150 \cdot (1-\varepsilon) \cdot \mu_f}{D_p} + 1.75 \cdot G \right)$$

where additionally to the variables defined underneeth equation (7)

Δl	m	flow path length in wick
ρ_B	kg/m³	fluid bulk density

Overall model and procedure for porous medium concept

The geometrical and load model of a subassembly is shown in Figure 8 and the insert with the porous layer in Figure 1 and Figure 2. The insert is assumed to extend over the total length. The subassembly is divided into several segments (slices). Input to the calculation are the helium pressure and temperature at the inlet, the desired coolant temperature rise, the surface heat load distribution and thereby the total mass flow rate.

The calculation starts with a first approximation of the pressure drop along the inlet duct assuming uniform outflow from the duct into the wick. With this axial pressure distribution, which serves as inlet pressure to the wick, the pressure drop in each slice of the wick is computed, leading to a first pressure distribution in the outlet duct. This must converge with the friction losses in the outlet duct that can be computed independently. The difference between these two pressure functions is used to redistribute the flow rates in the slices for further iterations.

After convergence has been reached, the pressure distribution in the inlet and outlet duct and the mass flow through the wick in each slice are known, and hence, all the other thermal-hydraulic variables. A typical pressure profile is shown in Figure 9 for illustration, along with normalised profiles of heat transfer coefficient and mass flow rate. It can be seen that the pressure drop in the inlet and outlet ducts contribute significantly to the total pressure drop in the subassembly. The flow rate and heat transfer coefficient turn out to be non-uniform with a variation of 6% for the HTC and 10% for the flow rate.

3.1.2.3 Equations and methods used for the multi-channel concept

The multichannel concept was analysed using a combination of thermohydraulic modelling by standard correlations and three-dimensional finite element simulation of the temperature distribution.

The correlations employed for the calculation of heat transfer coefficient and pressure drop are equations (1) and (2) displayed in 3.1.2.1. Temperature-dependent quantities in these correlations are evaluated at the average coolant temperature $T=T_{in}+0.5\Delta T$, with ΔT the overall coolant temperature gain; where maximum heat transfer coefficients are wanted, a coolant temperature of $T=T_{in}+\Delta T$ is used.

The division of mass flow between the central and lateral cold-leg channels was found by iterating until the pressure drops across the different channels are identical. Those mass flows were then used for determining the heat transfer coefficients h of all cooling channels.

A 3D finite element model using the commercial code FIDAP was built for structural temperature analysis, the main reason being that coolant temperatures in the hot and cold leg affect each other and that such a model does not require assumptions on the distribution of heat to the central and lateral inlet channels, which could affect estimated maximum temperatures significantly. The element grid in the cross-section of the model is displayed in Figure 3. Key features of the model are:

- the energy equation, but not the momentum equations, are solved for the fluid channels. Fluid velocities from the hydraulic model are used. A non-isotropic conductivity in the coolant, with large values perpendicular to the flow direction, is employed to achieve a representative flat temperature profile in the channel cross-sections;

- the inlet temperature of the rear channel is found as the mass-flow-weighted average of the central and lateral inlet channels. The collector bend between cold and hot leg is not modelled;

- interface elements that contain the heat transfer coefficients are modelled between channels and structure;

- the castellation of the plasma facing side has not been modelled. As a consequence, the distance of the FW surface to the heat sink, and the maximum temperature, could be slightly smaller than in the real case

- either perfect or no thermal contact was assumed between the inner channel wall and the cooling ribs provided by the flow channel insert.

The detailed finite element analysis was to costly to be carried out for every single operating point explored in this report. Instead, the finite element model was run for a few central cases, and the resulting maximum fluid and structural temperatures used to calibrate the parameters a and b in the model

$$T_{\max,wall} = T_{in} + a \cdot \Delta T_{cold\,leg,central} + b \cdot \frac{\overline{q}}{h}$$

for temperatures at the half way mark, i.e. the cross section of cold leg outlet and hot leg inlet.

The value a=1.3 reflects that the central channels see a higher heat flux than the lateral channels and that the Helium there is heated to about 30% above the nominal outlet temperature. Parameter b depends on the assumption of contact between the channel wall and the channel insert. In case of perfect contact, it is b=0.9, while for missing contact, b=1.25. Strictly, a and b change with ΔT and $\overline{q}$; however, the error is within ±50K, which is sufficient for assessing trends and understanding the larger picture.

3.1.2.4 Equations and methods used for the swirl rod insert concept

This concept is treated as a special case of the eccentric swirl promoter concept with zero eccentricity and just a single fin as sketched in Figure 4. As for all concepts, the insert is assumed to extend over the total length of the subassembly and the input to the calculation are the helium pressure and temperature at the inlet, the desired coolant temperature rise, the surface heat load distribution and thereby the total mass flow rate.

The heat transfer and pressure drop assessment is straightforward by use of equations (1) and (2) on page 13. The helical pitch of the fin for a full turn is assumed as 0.2 m. As was said earlier, the artificial 2D roughness has been ignored, instead a natural wall roughness of 1 micron is presumed in the pressure drop equations. In order to assess the channel wall temperature at the point of highest heat load (point E in Figure 23, see also the discussion in section 3.2 on page 21), a transverse peaking factor f_t = 1.2 is applied.

3.1.2.5 Equations and methods used for the eccentric swirl promoter concept

The geometrical model comprises a single subassembly with insert as shown in Figure 5, where all the dimensions are input parameters. Since the swirl promoter is twisted around its centre line the cross

sectional area of an individual sub-channel, and thus all the hydraulic quantities, vary periodically in longitudinal direction as illustrated in Figure 10. Therefore, the system of flow sub-channels is modelled as a 2D grid of $n_c \times n_z$ meshes, with n_c = number of sub-channels and n_z = number of axial meshes.

In order to calculate the heat transferred into the sub-channels we have to formulate the peripheral heat flux, q_s at the main channel inner wall for a given surface heat load incident at the subassembly. We use a modified chopped cosine function of the form

$$(9) \qquad q_s(\Phi) = \begin{cases} 0.5 \cdot \overline{q} \cdot f_t \cdot (1 + \cos(\xi \cdot \Phi)) & for \, |\Phi| < \pi / \xi \\ 0 & for \, |\Phi| \geq \pi / \xi \end{cases}$$

where Φ is the angle measured from the apex, and $\xi > 1$ forces the profile to be squeezed onto the region where $|\Phi| < \pi / \xi$, and $q_s(\Phi) = 0$ elsewhere. The transverse peaking factor, $f_t > 1$ can be chosen based on empirical results from thermal FE calculations. f_t is typically between 1.1 and 1.25, depending on the ratio of the subassembly width to channel diameter and on the material conductivity.

Once f_t has been set, ξ can be adjusted in a way that the integral underneath the curve $q_s(\Phi)$ is equal to the integral of the surface heat load $\overline{q} \cdot w_M$, that is

$$R \cdot \int_{-\pi}^{\pi} q_s(\xi \cdot \Phi) d\Phi = \overline{q} \cdot w_M$$

R is the radius of the channel inner wall. This equation can be solved for ξ after insertion of equation (9) and gives

$$(10) \qquad \xi = \frac{\pi \cdot R \cdot f_t}{w_M}$$

Starting with a given coolant temperature, pressure and mass flow rate at the entrance to the first row of meshes (which as a first approach is assumed to be evenly distributed among sub-channels), the pressure drop (equation (2)) and temperature rise (energy equation) in that row are calculated. In the same way the calculation proceeds through all axial meshes and determines the total pressure drop and temperature rise in each sub-channel. In equations (1) through (3) all variables are determined as function of z* instead of z, where z* is the length co-ordinate of the stretched-out helical sub-channels. Usually the resulting pressure drop will be different in each sub-channel and a few iteration steps with adjusted mass flow distribution are needed until pressure balance at the exit is reached.

3.1.2.6 Equations and methods used for the slot concept

From the modelling point of view this design is identical to the porous medium concept described in section 3.1.2.2, except for the porous medium layer, which in this case is a slot of typically 0.15 to 0.2mm width. Here the general equations for plain channels from section 3.1.2.1 (with roughness $R_t = 0.001mm$) have been used to determine pressure drop and heat transfer in the semi-peripheral slot flow. The slot in each axial slice is modelled as a single mesh and the fluid properties are taken at the mean temperature (inlet temperature plus half the nominal temperature rise). We are aware that the model can only be considered as a first approach since thermal-hydraulics in micro-channels are still subject to research.

The pressure drop in the inlet and outlet duct has also been calculated assuming a conical shape of the inlet duct and a ratio of cross sectional areas (inlet/outlet duct) of 10 at the entrance side and 1/10 at the exit. As to the iteration procedure, the description in section Overall model and procedure for porous medium concept on page 15 applies.

3.1.3 Thermal-hydraulic benchmarking of concepts

Applying the methodology from section 3.1.2 we have analysed the performance of the five divertor concepts in the parameter ranges defined in sections 3.1.1.1 and 3.1.1.2. Each concept offers several degrees of freedom to optimise the flow insert with respect to, e.g., pressure drop or heat transfer characteristics. Therefore a first screening was performed to demonstrate the sensitivity of the concepts to common and individual parameters and to find some preferred sets of insert parameters, like porous layer thickness for PM, size of central channel for MC, gap width for SRI and SLOT, eccentricity for ESP etc. Based on these results a systematic benchmarking was carried out using the most promising set of individual parameters for each concept and varying then the thermal-hydraulic and load parameters consistently. The results of this benchmarking is described below after summarising the procedure.

Benchmark procedure:

i.   Definition of a common reference geometrical and heat load model of a divertor subassembly according to Figure 8 with 2R=28mm, width=36mm, total length=heated length+2x0.1m.

ii.   For each concept chose the most promising insert geometry from screening calculations to fit into the subassembly model of step (i).

iii. Define a set of reference thermal-hydraulic parameters common to all concepts (as indicated below by the rich numbers)

iv.   Starting from the reference point defined in steps (i) through (iii) vary the thermal-hydraulic input parameters one by one through the following ranges

    a)   inlet pressure PIN = 8, 9, 10, 11, 12, 13, **14** MPa (7 points)

    b)   temperature rise DTF = **200**, 180, 160, 140, 120, 100 K (6 points)

    c)   inlet temperature TIN = 100, 200, 300, 400, 500, **600**, 700 °C (7 points)

    d)   average surface heat load = **3**, 4, 5, 6 MW/m^2 (4 points)

    e)   heated length = 0.5, 0.6, 0.7, 0.8, 0.9, **1.0** m (6 points)

v.   Perform the calculations outlined in section 3.1.2 for each of the 30 cases established in (iv) and plot the maximum wall temperature attained, $T_{E,structure}$, versus the power ratio, PR, where

    $T_{E,structure}$ = maximum structural temperature at fluid/structure interface within subassembly calculated from equation (13)

    PR   = ratio of circulator power (needed to force the fluid through the subassembly) to thermal power removed from subassembly.

vi.   For most concepts additional cases have been analysed to indicate trends when shifting the reference point to some other "centre point".

3.1.3.1 Benchmark results for the porous medium (PM) concept

The thermal-hydraulic performance of the PM concept when varying the parameters as outlined in the previous paragraph is depicted in Figure 11. Plotted is the maximum wall temperature within the subassembly, $T_{E,structure}$, as functions of the power ration, PR.

In the reference point, which is recognised as the origin of the set of branches in Figure 11, we read $T_{E,structure}$=880°C and PR=1%, very reasonable values. Please note that the maximum structural temperature at the outside of the channel is than this value, depending on the heat flux and wall thickness. This however is generic to all concepts and has thus not been considered here.

The different branches in the figure indicate the impact of varying the main parameters one by one while keeping the others at their reference value.

Branch (a) represents the reduction of the system pressure from 14 to 8 MPa in increments of 1 MPa. It is seen, that $T_{E,structure}$ does not change at all, since the heat transfer coefficient is independent of system pressure under these conditions. On the other hand, the power ratio increases from 1 to 3% within this pressure range. the markers on curve (a) are not equidistant (whereas the pressure

increments are), indicating that further pressure reduction to below 8 MPa penalises the pumping power very strongly.

Curve (b) shows the impact of reducing the fluid temperature rise, ΔT, in the subassembly from 200K to 100K in steps of 20K. One can see that up to 100K can be saved in $T_{E,structure}$ but at the expense of a sharp increase in power ratio to PR=6.5%. Nevertheless, this may still be acceptable for power conversion of the divertor heat.

Curve (c) with variation of the coolant inlet temperature between 100°C and 700°C with the reference point at 600°C has only been included to demonstrate the strong influence on $T_{E,structure}$ and at the same time on a benefit in pumping power. As was said in section 3.1.1.1 on page 11 a coolant temperature below 600°C does not seem to be acceptable for refractory materials. Yet, curve (c) visualises the importance of establishing a proper coolant temperature window in divertor design for a power plant.

Curve (d) illustrates the temperature vs. power ratio behaviour if the average surface heat load is increased from 3MW/m^2 to 6MW/m^2 in increments of 1MW/m^2. While $T_{E,structure}$ rises moderately by about 90K, the power ratio goes up by a factor of 3.5 ending at 3.5%, which is still reasonable. Hence, from the thermal-hydraulics point of view an average heat load of 6MW/m^2 or even higher seems to be manageable with a high-pressure system. The limit is set by mechanical constraints as will be discussed in section 3.2.

Finally, curve (e) indicates the influence of the heated length or channel length. As expected, the power ratio scales almost linearly with the heated length. A slight increase of the structural temperature is observed for small lengths.

In order to broaden the view for the PM concept, the same exercise has been repeated for several other "centre" points (Figure 12). Here, Figure 11 has been reproduced in the upper left frame for comparison. The other plots show the results obtained, when changing, e.g., the reference pressure from 14 to 8MPa, or the average surface heat load from 3 to 6 MW/m^2, or the thickness of the porous layer. The two last plots are examples for non-uniform heat load profiles, i.e., triangular profiles with a peak heat load of twice the average load. In principle the same trends can be observed as discussed with Figure 11 but with different intensities.

3.1.3.2 Benchmark results for the multi-channel concept

The thermal-hydraulic performance of the MC concept under parameter variations according to the benchmark procedure is displayed in Figure 13. For these calculations, the cross section of the MC concept was scaled down to a width of 36 mm, with the channel diameter of 28 mm and the channel insert diameter 18 mm. As before, the maximum temperature at the inside channel wall and the circulator power ratio are used as figures of merit for the operating regime.

The reference point at the origin of the set of branches is 1130°C at PR=3.2%. Even in the optimistic case of perfect contact of channel and channel insert, the largest temperature difference across the channel is about 1130°C - 800°C = 330 K. The implied mechanical stresses are likely to exceed admissible values, as was found in [2].

The other branches in the diagram suggest that there is limited scope for improvement. The Helium pressure of 14 MPa (branch a) is needed to stay at moderate PR. A reduction of Helium temperature increase (b) would reduce structural temperatures but would push up the PR significantly. A reduction of inlet temperature (c) by a moderate value would be an efficient way of shedding the temperature maximum.

The effect of a surface heat load increase to 6 MW/m^2 is a PR increase to PR = 10.7%. While this value could still be acceptable, the rise of the channel wall temperature to $T_{max,wall}$ = 1195°C implies even larger stresses than in the reference case. Also, at the chosen operating point, a reduction of the heated length would benefit the PR but would strongly raise structural temperatures by means of reduced mass flows and reduced heat transfer coefficients.

A broader view of the MC concept is supported by Figure 14, where the top figure is identical to Figure 13. The performance data plotted in the middle highlight the adverse effect that a missing contact of channel and channel insert ribs would have on the maximum channel wall temperature. The

bottom figures displays parameter variations about the operating point suggested in [2]. Regarding structural temperatures, this operating regimes are better suited than the values above. However, the present PR calculations (the discrepancies with [2] were mentioned in 3.1.2.3) as well as the point for a temperature rise of 200K made in 3.1.1.1 disallow the operation at this operating point.

3.1.3.3 Benchmark results for the swirl rod insert (SRI) concept

The thermal-hydraulic performance of the SRI concept is shown in Figure 15 on page 36. As in previous cases curves (a) to (e) represent the parameter changes defined in section iv on page 18 with the reference point as origin of the branches. The width of the annulus has been chosen as 2.2mm from the screening study. The outer diameter of the channel and the assembly width are 28mm and 36mm, respectively.

At the reference point we read a maximum structural temperature at the fluid/structure interface of 1170°C, that is 290K higher compared to the PM concept. Also the power ratio is significantly larger, reaching 2.5% compared to 1%. In general, all curves are shifted toward a higher temperature level and are stretched out on the power ratio scale relative to the performance of the PM concept.

There is a remarkable dependency from heated length (curve e), which is typical for designs with mainly longitudinal flow pattern. Hence, the power ratio becomes less of a concern for small lengths but the temperature in the structure does.

The performance becomes even worse when altering the centre point in a way it was done with the PM concept (Figure 16). It must be repeated that a key feature of the SRI concept, the longitudinal grooves for heat transfer enhancement, has been ignored (like with all the other concepts) in this assessment.

3.1.3.4 Benchmark results for the eccentric swirl promoter (ESP) concept

The ESP concept performs somewhere in the middle when compared to the other concepts (Figure 17). This can best be seen in an overlay plot of all concepts studied (Figure 21), always taken the diagrams with the common reference point as origin.

The maximum structural temperature amounts to 1080°C at a power ratio of 2.3%. $T_{E,structure}$ is insensitive against the system pressure (as with all concepts, curve a) and only very little changing with the average surface heat load (curve d in Figure 17). On the other hand, the power ratio is much more sensitive to deviations from the reference point than the PM concept. This is common and inherent to all designs with longitudinal flow as opposed to the cross flow concepts PM and SLOT.

Additional cases have been investigated similar to the procedure given for the PM concept. The plots are shown in Figure 18, again Figure 17 reproduced in the upper left corner for comparison. At a system pressure of 8MPa (top right) there is no freedom to lower the temperature rise below 200K (curve b) or increasing the heat load to above 3MW/m² (curve d). A similar picture is obtained if the centre point is at high pressure and high heat load (centre left). There is some potential for improvement in power ratio by fine-tuning the geometrical parameters like eccentricity and number of fins, as the example with eccentricity of 0.15mm instead of 0.2mm indicates (centre right). The two cases at the bottom of Figure 18 with a peaked power profile up to 6MW/m² yield rather high temperature levels centred at 1300°C, which may be too high to cope with thermal stresses, in particular at reduced heated lengths (curve e).

3.1.3.5 Benchmark results for the slot concept

The thermal-hydraulic performance of the SLOT concept shows a remarkably different behaviour compared to the other concepts (Figure 19). It is characterised by an extremely low power ratio (0.7% at the reference point) and a substantial reduction of the maximum structural temperature with reduced coolant ΔT from 200K to 100K (curve b). Also the variation of the power ratio with system pressure is extremely small (curve a). A further unique feature is that the structural temperature level tends to go down with increasing average heat load (curve d). This is explained by the fact that the gain in calculated heat transfer coefficient overcompensates the larger film ΔT. As was said in section 3.1.2.6, there are reservations with regard to the formalism applied to this micro-channel geometry. Overall, the system is attractive at moderate coolant temperature rise of about 100K.

20

Further cases with modified centre points of the parameter set are depicted in Figure 20 in the same pattern as presented for the other concepts and the relatively small power ratio is evident (compare also Figure 21).

3.1.4 Conclusion of thermal-hydraulic assessment

The thermal-hydraulic assessment has focussed on a comparison of the maximum structural temperature at the fluid/structure interface at any point of the subassembly, and on the power ratio for a given set of operating parameters. These two quantities implicitly include the other parameters of concern in designing high heat flux components, i.e., the heat transfer coefficient, fluid velocities and pressure loss, and are therefore regarded as appropriate indicators for the thermal-hydraulic performance of different concepts. Table 7 summarises these quantities at what we called the reference point, that is the reference set of operating parameters as defined in section 3.1.3 on page 18. Variations of the operating conditions are compared in Figure 21, which is an overlay of the plots produced for the individual concepts in subsections 3.1.3.1 through 3.1.3.5.

Striving for low maximum wall temperature and low power ratio it is clearly seen that the PM concept performs best, followed by the SLOT concept. The reason for the low temperature level is the fact that the heated side of the channel is supplied with coolant at inlet temperature over the entire channel length. However, the calculation models adopted imply the largest uncertainties, namely for the PM concept with regard to the unproved heat transfer coefficient produced by the porous medium (see the discussion in section 3.1.2.2), and for the SLOT concept because of its micro-channel nature (section 3.1.2.6). The concepts with longitudinal flow (ESP, SRI and MC) behave similar in terms of power ratio. Differences are seen in the temperature level with the ESP performing best. Further heat transfer enhancement by surface roughening and/or by thermal conduction in ribs (ESP and MC) may alter the picture somewhat.

Table 7: Comparison of concepts performance at reference point

Divertor type	Max fluid/structure interface temperature (°C)	Ratio of pumping power to thermal power (%)
Porous medium (PM) concept	880	1
Multi-channel (MC) concept	1240	2.3
Swirl rod insert (SRI) concept	1170	2.5
Eccentric swirl promoter (ESP) concept	1080	2.3
Slot (SLOT) concept	1090	0.7

3.2 Thermal stress considerations

A firm stress analysis for the divertor concepts investigated is beyond the scope of this study, although it has been shown in the recent study of the porous medium concept that thermal stresses are a dominating factor in establishing the performance limits of a certain design. It was also demonstrated that a reasonable stress assessment can only be made by means of a coupled thermal-hydraulic-mechanical analysis for well defined design and operating conditions. This is not the objective of the present study. Nevertheless, the thermal-hydraulics and the flow pattern of a given system determine to a large extent the operating temperature level of the divertor structure as well as gross temperature gradients within a given cross section of the channel assembly. Hence, these two quantities can serve as indicators in a comparison of different designs with view to their mechanical behaviour. The temperature level has been discussed in the previous section, the temperature gradient will be addressed below.

It is believed that the five concepts analysed here can essentially be made identical in their outer channel structure, i.e., a mono-block type bar with a cylindrical bore (with or without a lining tube to meet the double containment principle), a protection layer at the plasma facing surface, made of the

same material and of almost the same size. Only the inserts are different, which do not significantly interact with the outer structure mechanically. Then a suitable indicator for the thermal stress level, given that no bending of the beam be allowed, is the temperature difference between the front and back side of the beam. We choose two positions, i.e. the axis-parallel lines through points C at the armour/structure interface and F of the channel wall (Figure 23), and determine the maximum of this temperature difference of all cross sections along the channel length,

$$(11) \qquad \Delta T_{C-F} = \Delta T_{C-E} + \Delta T_{E-F}$$

with point E of the plasma-facing channel wall. This quantity will then be used as thermal stress indicator. The procedure will be done at first for a uniform heat load distribution and subsequently for a peaked heat load profile.

ΔT_{C-E} is the temperature difference through the structure between structure/armour interface and cooling channel. This definition assumes that the armour is castellated or of a so-called "brush" type and has no significant impact on the thermal stresses within the structure. ΔT_{C-E} can be expressed by

$$(12) \qquad \Delta T_{C-E}(z) = \frac{f_t \overline{q}}{k} s$$

$f_t =$ transverse peaking factor, i.e. ratio of heat flux at point E to average incident surface heat flux $\overline{q}(z)$ at some axial location z

$\overline{q}(z) =$ average incident surface heat flux to divertor assembly at some axial location z

$k =$ thermal conductivity of structural material
$s =$ wall thickness

3.2.1 Uniform heat load

ΔT_{E-F} is easily determined for the five divertor concepts, if we assume uniform heat flux distribution along the channel axis, z, namely

$$\Delta T_{E-F} \equiv T_{E.structure} - T_{F,structure}$$

where the temperature in the structure along the line through point E, $T_{E,structure}(z)$, is simply

$$(13) \qquad T_{E,structure}(z) = \frac{f_t \overline{q}}{h(z)} + T_{E,coolant}(z)$$

$h(z) =$ heat transfer coefficient between channel wall and coolant

$T_{E,coolant}(z) =$ bulk coolant temperature at E

At the back side of the channel we can assume zero or negligible heat flux, thus

$$T_{F,structure}(z) = T_{F,coolant}(z)$$

Altogether, we obtain for the temperature difference

$$(14) \qquad \Delta T_{E-F}(z) = \frac{f_t \overline{q}}{h(z)} + T_{E,coolant}(z) - T_{F,coolant}(z)$$

Figure 23 shows schematically how the structural and coolant temperatures evolve along the channel axis in case of uniform heating. For the PM and SLOT concepts we have $\Delta T_{E-F}(z) = const$ and also the structure temperatures in E and F are constant. For the SRI and ESP concepts we also find approximately $\Delta T_{E-F}(z) = const$ but with rising temperature level. Only for the MC concept $\Delta T_{E-F}(z)$ increases linearly, reaching its maximum at the channel outlet.

The temperature difference of the coolant between E and F (the term $T_{E,coolant}(z) - T_{F,coolant}(z)$ in the last equation) is practically zero at the outlet for the three concepts MC, SRI and ESP, and it is equal to the negative mean coolant temperature rise in the assembly for the PM and SLOT concepts, ΔT.

With the two temperature differences defined, we can rewrite ΔT_{C-F} for the five concepts as listed in Table 8, centre column.

3.2.2 Non-uniform heat load

If the heat load is peaked as is usually the case in divertor application, namely in poloidal direction of the torus (that is in axial direction of the divertor subassemblies) the assessment is not as straightforward as in the uniform case. It then depends on the profile where the critical cross section in terms of thermal stresses is. For the special case that the heat load has its maximum half way of the heated length and is symmetric, a reasonable approximation of equation (14) can be formulated for the cross section with maximum load. The results are also given in Table 8, right column, without derivation. The additional variable f_a is the axial peaking factor, the ratio of peak incident heat load to average incident heat load to the divertor assembly.

Table 8: Thermal stress indicator for divertor concepts

Concept	Equation (11) for uniform heat load	Equation (11) for axially peaked heat load
Porous medium (PM)	$\Delta T_{C-F} = f_t \overline{q}(\frac{1}{h} + \frac{s}{k}) - \Delta T$	$\Delta T_{C-F} = f_a f_t \overline{q}(\frac{1}{h} + \frac{s}{k}) - f_a \Delta T$
Multi-channel (MC)	$\Delta T_{C-F} = f_t \overline{q}(\frac{1}{h} + \frac{s}{k})$	$\Delta T_{C-F} = f_a f_t \overline{q}(\frac{1}{h} + \frac{s}{k}) - 0.5\Delta T$
Swirl rod insert (SRI)	$\Delta T_{C-F} = f_t \overline{q}(\frac{1}{h} + \frac{s}{k})$	$\Delta T_{C-F} = f_a f_t \overline{q}(\frac{1}{h} + \frac{s}{k})$
Eccentric swirl promoter (ESP)	$\Delta T_{C-F} = f_t \overline{q}(\frac{1}{h} + \frac{s}{k})$	$\Delta T_{C-F} = f_a f_t \overline{q}(\frac{1}{h} + \frac{s}{k})$
Slot concept (SLOT)	$\Delta T_{C-F} = f_t \overline{q}(\frac{1}{h} + \frac{s}{k}) - \Delta T$	$\Delta T_{C-F} = f_a f_t \overline{q}(\frac{1}{h} + \frac{s}{k}) - f_a \Delta T$

It can be seen from the table that the PM and SLOT concept, in principle, perform best because they have the coolant temperature rise, ΔT, subtracted on the right hand side of the equations. The others rank equally in case of uniform heat load. For peaked heat load profiles the situation is similar with some advantage of the MC concept over SRI and ESP. However, this would be true only if the heat transfer coefficient, h, was equal for all concepts, which is not the case. Taking the different values of h for a certain set of thermal-hydraulic parameters into account, the picture might change. For example, Figure 22 shows the dependency of ΔT_{C-F} from the heat transfer coefficient for uniform (top) and peaked (bottom) heat load profiles, and the markers on the curves indicate the actual h values pertaining to individual concepts for the thermal-hydraulic parameters mentioned in the figure caption. Here we see that the smallest structural temperature difference, ΔT_{C-F}, is obtained with the PM concept, whereas the advantage of the SLOT concept relative to MC, SRI and ESP is marginal due to its poor heat transfer coefficient.

The temperature difference ΔT_{C-F} can be used as a stress indicator by relating it to the the simple case of a uniform bar of rectangular cross section that has one face at a uniform temperature T and the opposite face at a uniform temperature T+ΔT^*, with a linear temperature profile. For that case, with fixed ends holding the bar straight, Young [11] quotes a maximum bending stress σ of

(15) $$\sigma = \tfrac{1}{2}\alpha E \Delta T^*$$

E	Youngs modulus of structural material
α	Thermal expansion coefficient of structural material
ΔT^*	Structural temperature difference across the divertor subassembly

Using data for tungsten with $\alpha =5.3\times10^{-6}$ 1/K and $E =3.62\times10^5$ MPa, we obtain for any 100 K of ΔT_{C-F} a thermal stress of about 100 MPa. This rule of thumb shows good agreement with the case of a 3-point tungsten support structure analysed in [1] by finite element analysis for the PM concept. However, when material strength bv

For tungsten alloy, the allowable stress levels are of the order of 300 MPa at 1100 to 1200 °C. In other words, any operational state with a ΔT_{C-F} of about 300 K produces acceptable stress levels. It follows from this rough estimate with reference to Figure 22 that only the PM concept would have the potential to cope with the thermal stresses under the conditions presumed in this example, provided the heat transfer coefficient of at least 15000 W/(m^{2}K) can be realised for the PM design.

A general measure to alleviate thermal stresses would be to allow some bending of the subassemblies as was investigated in [1].

3.2.3 Comments on divertor performance limits

With the limits on divertor performance so important for the design of the overall fusion plant, it is obvious that a statement on the capability of the present concepts is expected by the reader. In a draft of this report, there were indeed considerations included on the limits of the PM divertor. However, there have been a number of reasons to remove that section and carry out a more thorough study than would have been possible in the framework of this report:

1. The motivation for this report has been a comparison of divertor concepts from the PPCS on a level playing field, i.e. unifying boundary conditions without making changes to the designs. Thus, the data provided in this report are relevant in comparing the designs, but they do not reflect the kind of optimised design that would be required for the considerations of performance limits.
2. The allowable stress limits applied in the preparatory phase of the PPCS were for un-irradiated tungsten in stress-relieved conditions. However, the re-crystallisation temperature may be reduced by neutron irradiation to a value below the operating temperature. In this case it would be very difficult not to exceed the stress limits. It remains to be seen whether W-alloys can be developed with a re-crystallisation temperature guaranteed to stay above the maximum operating temperature of the structure under irradiation.
3. Finally, for the PM concept that appears to be the most promising of the five considered performance predictions carry a large uncertainty, because experimental experience and empirical correlations are based on a copper/water system rather than tungsten/helium. Under these circumstances, the design cannot be optimised confidently. As an alternative approach it has been proposed to optimise the SLOT concept instead: this task can be done today, using standard correlations (which are known to be conservative for the micro-channels approached by very thin slots, where measurements suggest a HTC rise of up to 30%), and taking the results as a lower boundary for the presumed superior PM concept.

More work on divertor optimisation and performance limits will be carried out and reported in the framework of the PPCS.

3.2.4 Conclusions from simplified stress assessment

Thermal stresses in combination with operational temperature windows for structural materials are the limiting factor for all divertor concepts considered, with the best inherent potential assigned to the porous medium concept.

The SLOT design, from its principal configuration equivalent to the PM concept, does not show significant advantage compared to the others, unless the predicted heat transfer in the micro-slot can be strongly enhanced.

The concepts with predominantly axial flow like ESP, MC and SRI do not show large differences related to thermal stress (with small advantages for ESP) and have a chance only at moderate (say 3 MW/m^2) and almost uniform heat loads.

Peaked heat load profiles with axial peaking factors greater than 1.5 to 2 tend to drive thermal stresses excessively up, unless some bending of the divertor subassemblies can be allowed.

4 Proposal of key elements of a reference divertor design

The aim of this report is to apply identical operating conditions to the different Helium cooled divertor concepts, and, by this comparison, to understand the relative merit and scope of the concepts. The choice of operating conditions was guided by considerations of commercial operation. Great care has been taken to select evaluation criteria that are clear and simple yet incorporate the important information of structural temperature and temperature differences, thermal stresses and power conversion efficiency that underlies the determination of a heat flux limit for any divertor concept.

From the results reported, conclusions can be drawn about the key characteristics of a successful divertor design.

1. **Large heat transfer coefficient:** This requirement is obvious yet needs a balanced discussion of concepts. Concepts using longitudinal flow (MC, SRI, ESP) have to find a balance between heat transfer capability and pressure drop. Methods of promoting flow swirl would act in the same direction, raising both HTC and pressure drop, and would only allow a limited optimisation of the concept. Concepts featuring transversal flow through the divertor (PM, SLOT) appear to have more scope for large HTC. Since this value is limited to the short stretch of flow where it is needed, the impact on overall pressure drop is small. Other than straight flow channels, these concepts are understood to a lesser extent, particularly regarding the theoretical analysis and their behaviour under realistic conditions and sizes of the divertor application.

2. **Delivery of low-temperature coolant to the First Wall:** In the analysis it stands out that transversal flow concepts deliver coolant of the same low temperature all along the length of the divertor, thus keeping the overall temperature level low. Longitudinal-flow concepts have structural temperature rise about linearly over the length of the divertor, focussing the most severe mechanical conditions (material properties are temperature-dependent) on the location of maximum temperature.

3. **Use of refractory materials:** At the divertor temperatures and stresses encountered, refractory metals are probably the only feasible material.

These conclusions support the exploration of transversal-flow concepts. They must not hide, though, that the behaviour of such concepts under divertor conditions, their cooling capability under thermal load, their sensitivity to peaked power profiles, their scaling to divertor size need to be investigated and pose a higher development risk than longitudinal divertors.

5 Conclusions and further work

This report has assessed a number of Helium cooled divertor concepts based on a common set of operating conditions, and using both thermohydraulic performance and maximum stress as criteria. Despite having been kept very general, the key divertor feature recommendations suggest that most of the concepts investigated have little potential for high levels of heat flux. On the other hand, they imply that micro-channel and jet impingement schemes that could not be evaluated here could be candidates for a high heat flux divertor.

While all the concepts compared had a performance tag attached in the preparatory analyses, the assessing nature of the present report has not allowed to go beyond these data and seriously re-iterate the issue. However, within the third phase of the PPCS divertor work will focus on a slot design (for the reasons given in point 3 of section 3.2.3), with the goal of pushing the performance towards 10 MW/m^2.

References

[1] K. Kleefeldt, S. Gordeev: Performance limits of helium-cooled divertor (unconventional design), Final Report on Subtask PPA1.3.2, FZKA-6401, Mar 2000).

[2] M. Ferrari: Thermal-hydraulic study for a channel He cooled divertor, ERG/FUS/TN RTI/PPA/DIV/003-99 (Dec 1999).

[3] C.B. Baxi, C.P.C. Wong: Review of helium cooling for fusion reactor application, Proc. of ISFNT-5, Rome, 19 – 24 Sept. 1999, M.A. Abdou (Editor), Fusion Engineering and Design, 51-52 (2000) 319-324

[4] K. Kleefeldt: The eccentric swirl promoter as an alternative to twisted tapes in high heat flux components, unpublished.

[5] S. Malang, H. Schnauder, M. Tillack: Combination of self-cooled liquid metal breeder blanket with a gas turbine power conversion system, Fus. Eng. Des. 41 (1998) 561-567.

[6] VDI-Wärmeatlas, Berechnungsblätter für den Wärmeübergang, 4. Auflage 1984.

[7] J.E. Lindemuth, D.M. Johnson, J.H. Rosenfeld: Evaluation of porous metal heat exchangers for high heat flux components, ASME Winter Annual Meeting 1994.

[8] B. Eck: Technische Strömungslehre, Siebente neubearbeitete Auflage, Springer-Verlag, Berlin/Heidelberg/New York, 1966.

[9] D.L. Youchison et al.: Thermal performance and flow instabilities in a multi-channel, helium-cooled, porous metal divertor module, Fus. Eng. Des. 49-50 (2000) 407-415.

[10] G Campbell et al.: Hexagonal array microchannels for plasma-facing components. Personal communication, Saddleback Aerospace, Los Alamitos, CA 90720, USA.

[11] W.C.Young: Roark's Formulas for Stress & Strain, 6th ed., McGraw-Hill, New York, 1989.

[12] Plansee Aktiengesellschaft: Tungsten product specification, 39.39.50-GR130, 1997.
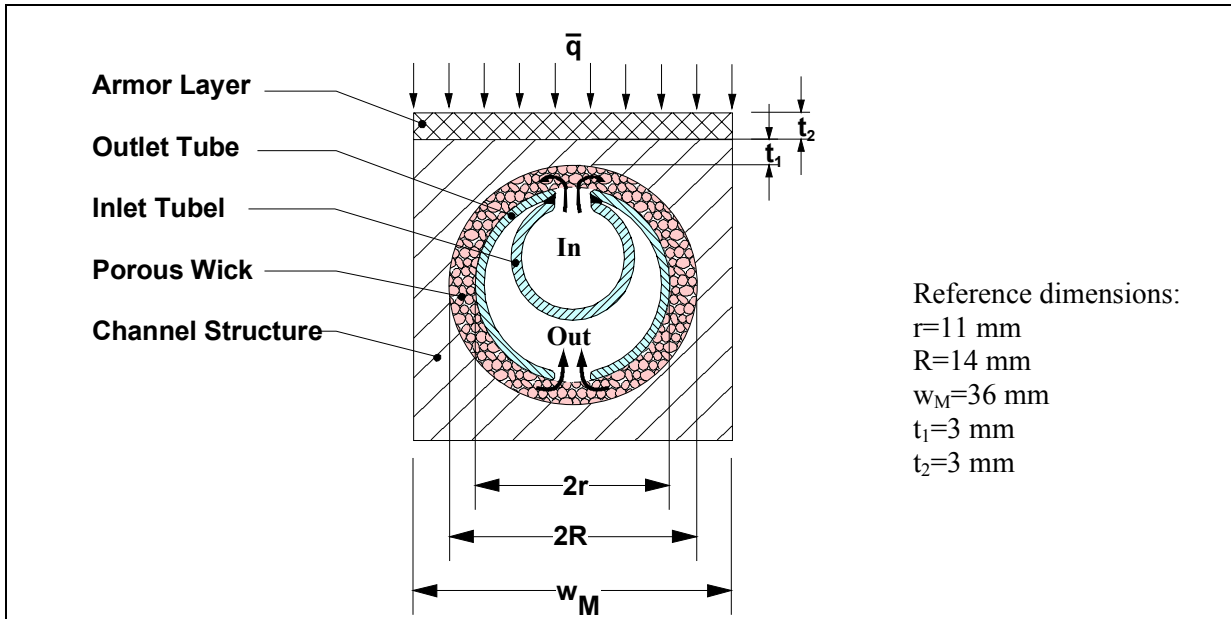
Figure 1: Typical cross section of a porous media target plate channel
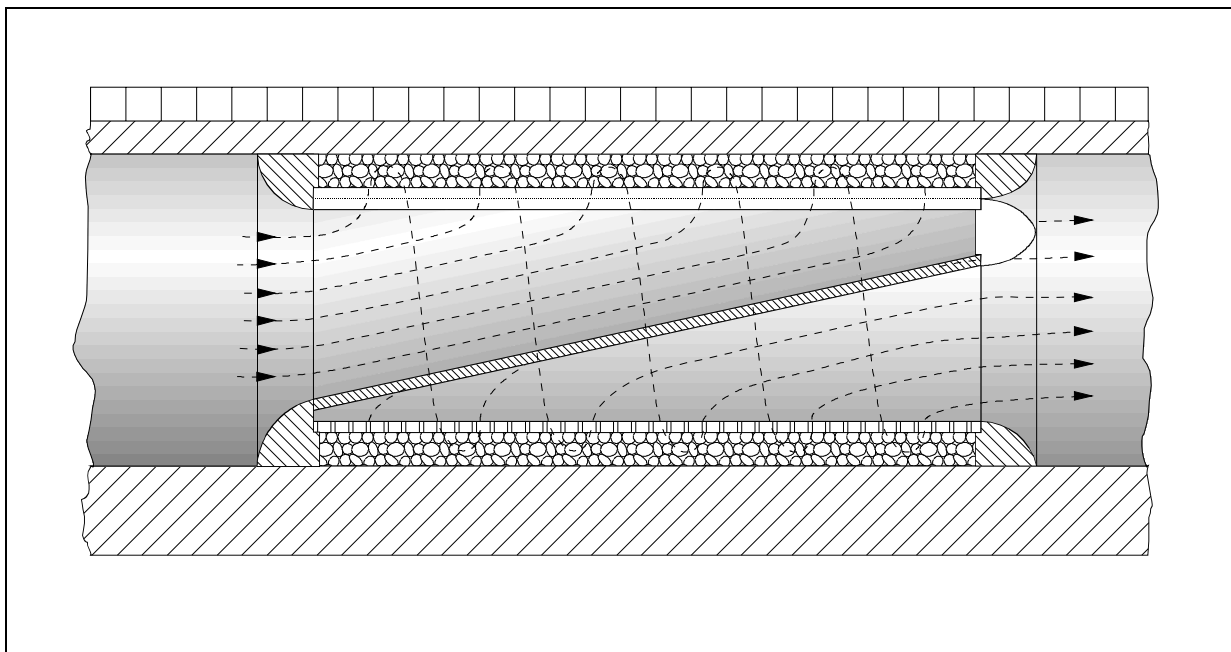
Figure 2: Longitudinal section through target plate channel (length scaled-down by 1/10)
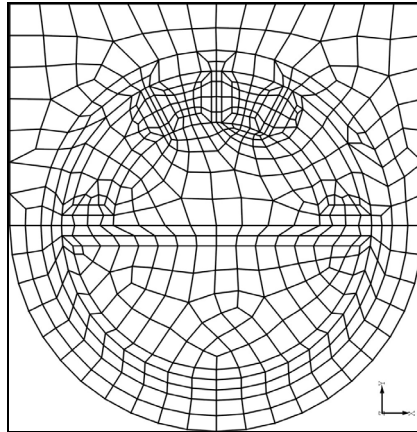
Figure 3: Multichannel concept, cross section of the grid used in finite element analyses
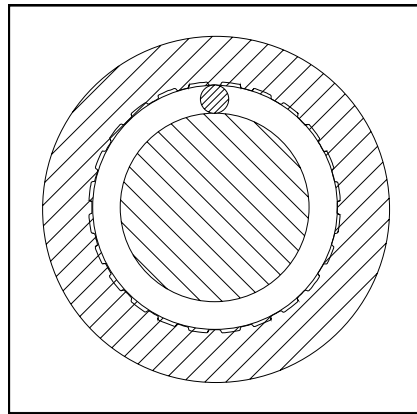
Figure 4: Swirl rod insert concept, Dimensions see
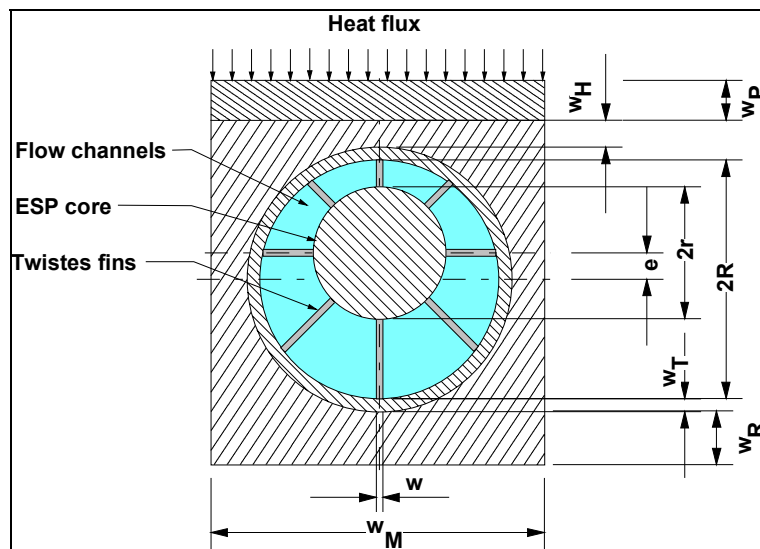
Figure 5: Eccentric swirl promoter concept, nomenclature
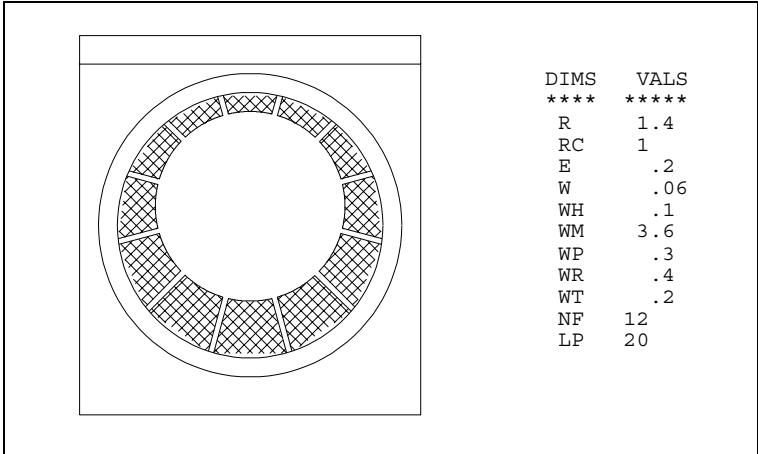
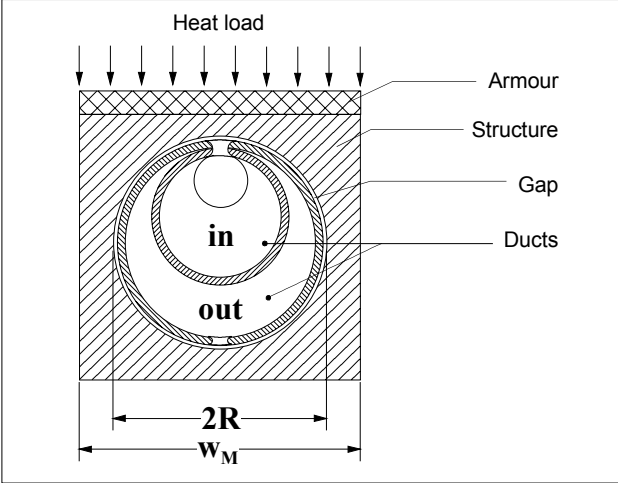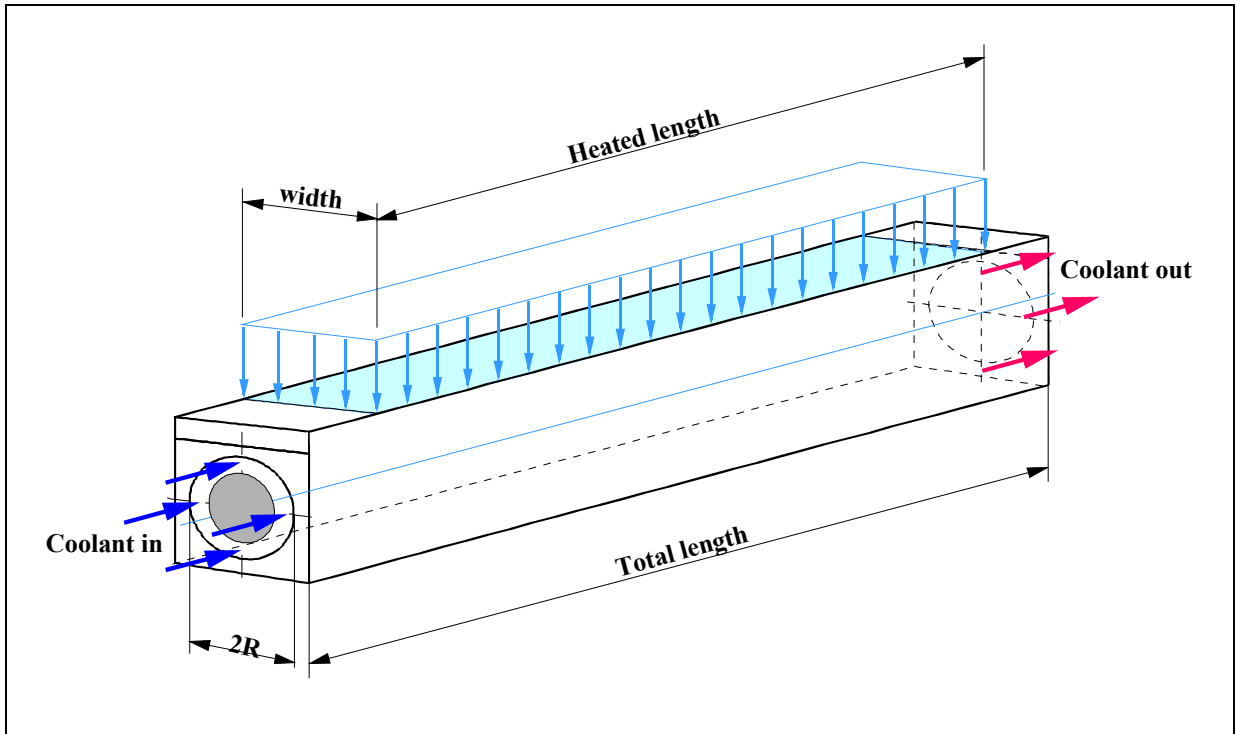**Figure 6: Eccentric swirl promoter, reference dimensions in mm**

Figure 7: Slot concept with tapered inlet duct

Figure 8: Geometrical and heat load model of divertor subassembly
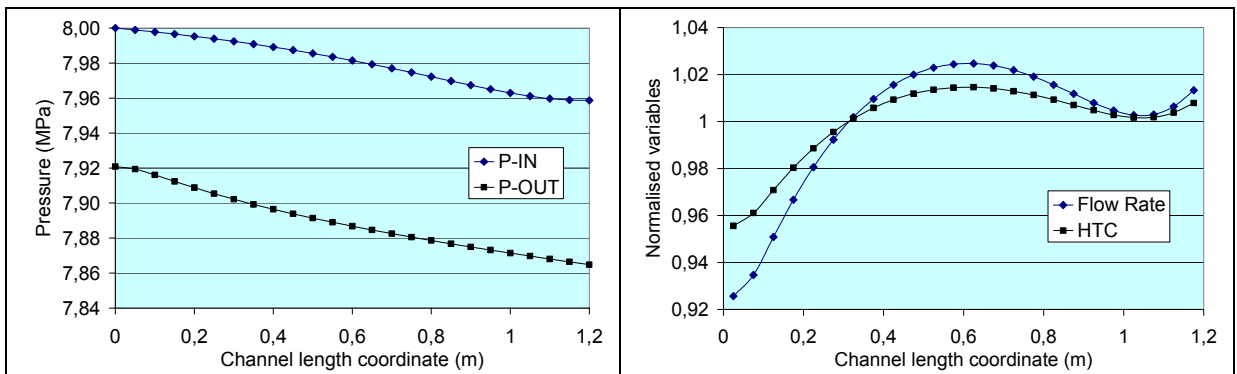
Figure 9: Typical profiles of thermal-hydraulic variables in the porous medium concept

P-IN and P-OUT are the pressure in the inlet and outlet duct, respectively. The difference between both is the pressure drop in the porous layer. The flow rate and heat transfer coefficient profiles shown in the right frame are normalised to their mean values.
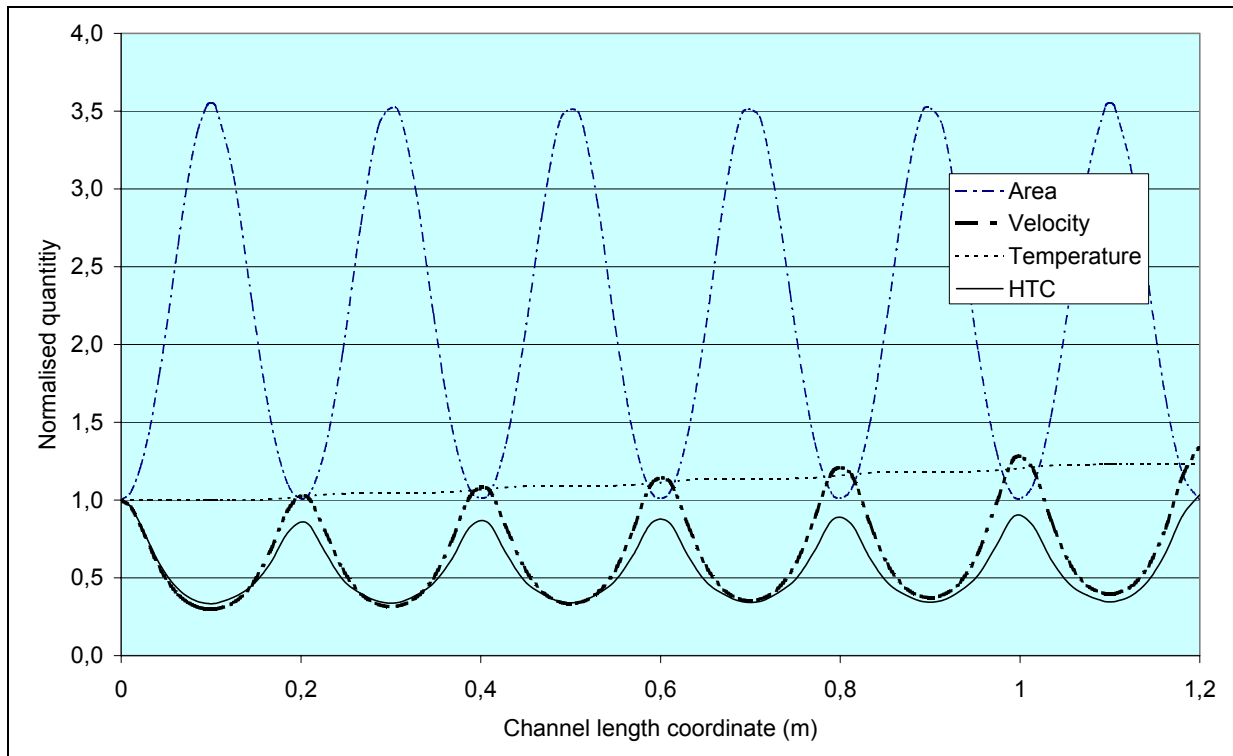
Figure 10: Typical profiles of thermal-hydraulic variables in the ESP concept

Quantities are normalised to their value obtained at the entrance to the subassembly (length co-ordinate = 0). The cross section area of a sub-channel varies by a factor of 3.5 while it winds around the eccentric core with a pitch of 0.2 m. Accordingly, the velocity oscillates in contra-phase with a slight increase in the peak values caused by the stepwise increase in coolant temperature. The heat transfer coefficient is in phase with the velocity showing insignificant gross changes.
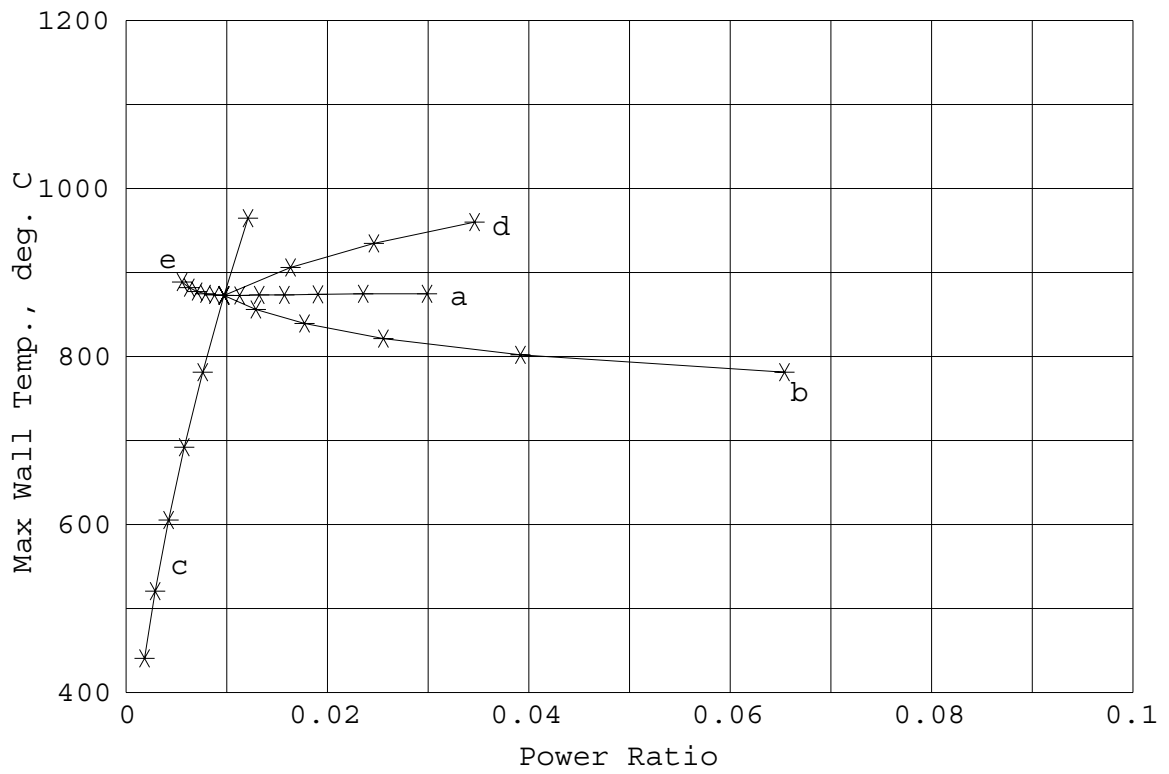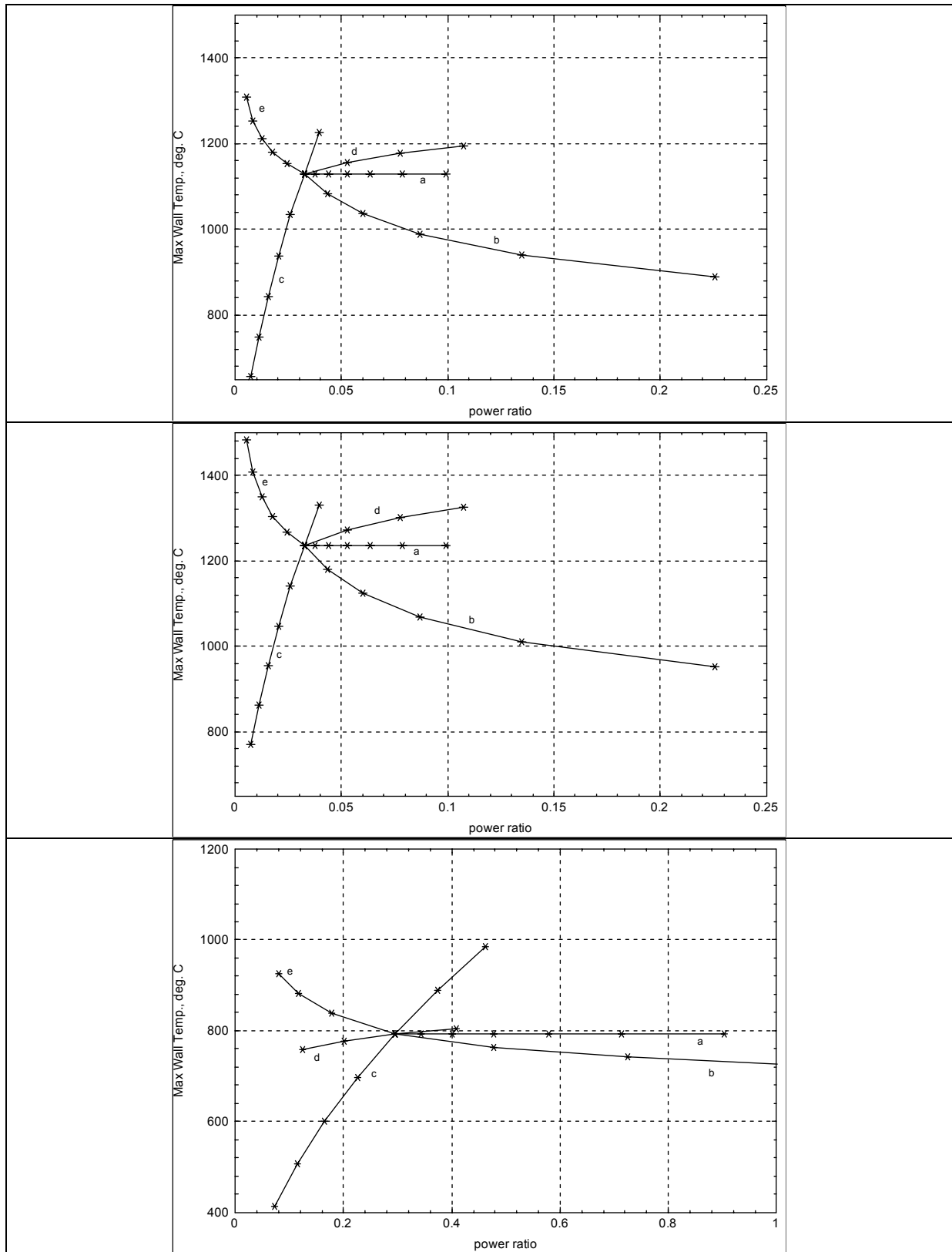
Figure 11: Thermal-hydraulic performance of the porous medium concept

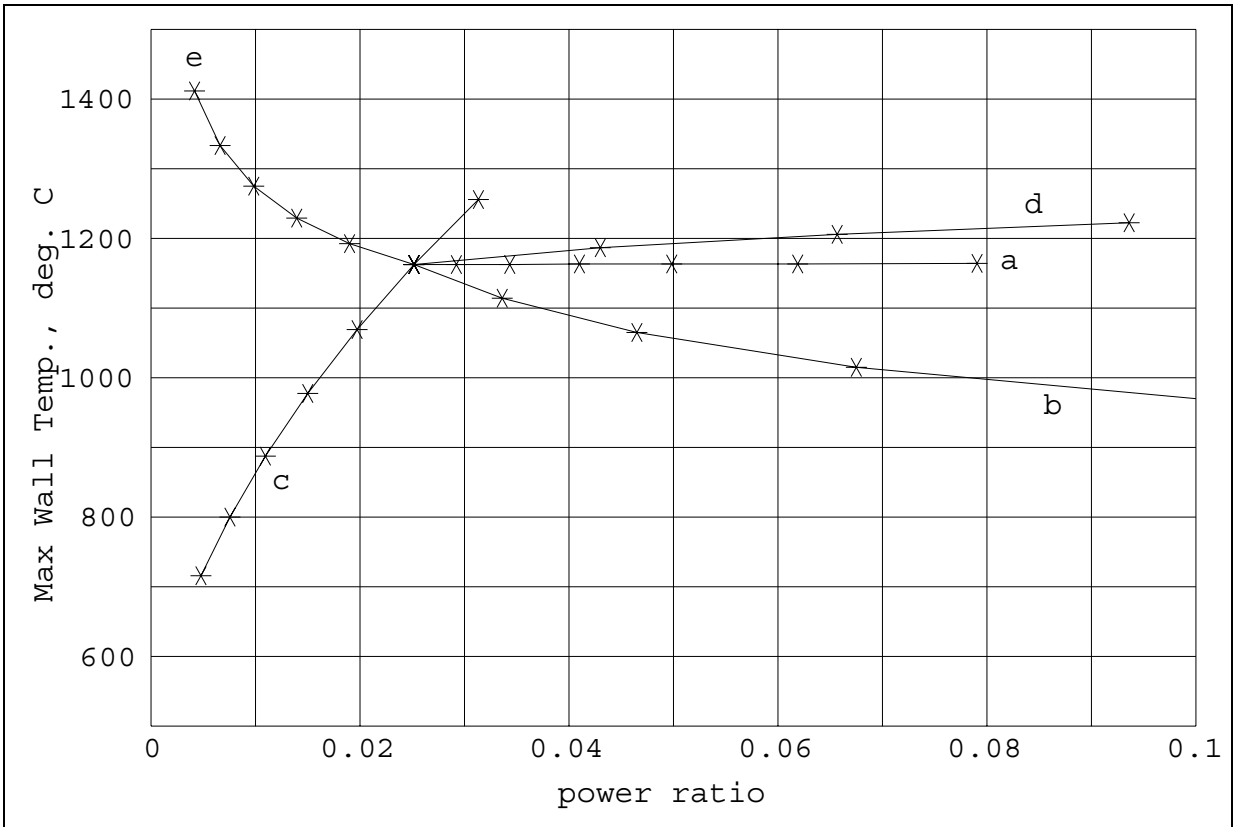(Curves a, b, c, d, e refer to parameter ranges defined in paragraph iv on page 18)
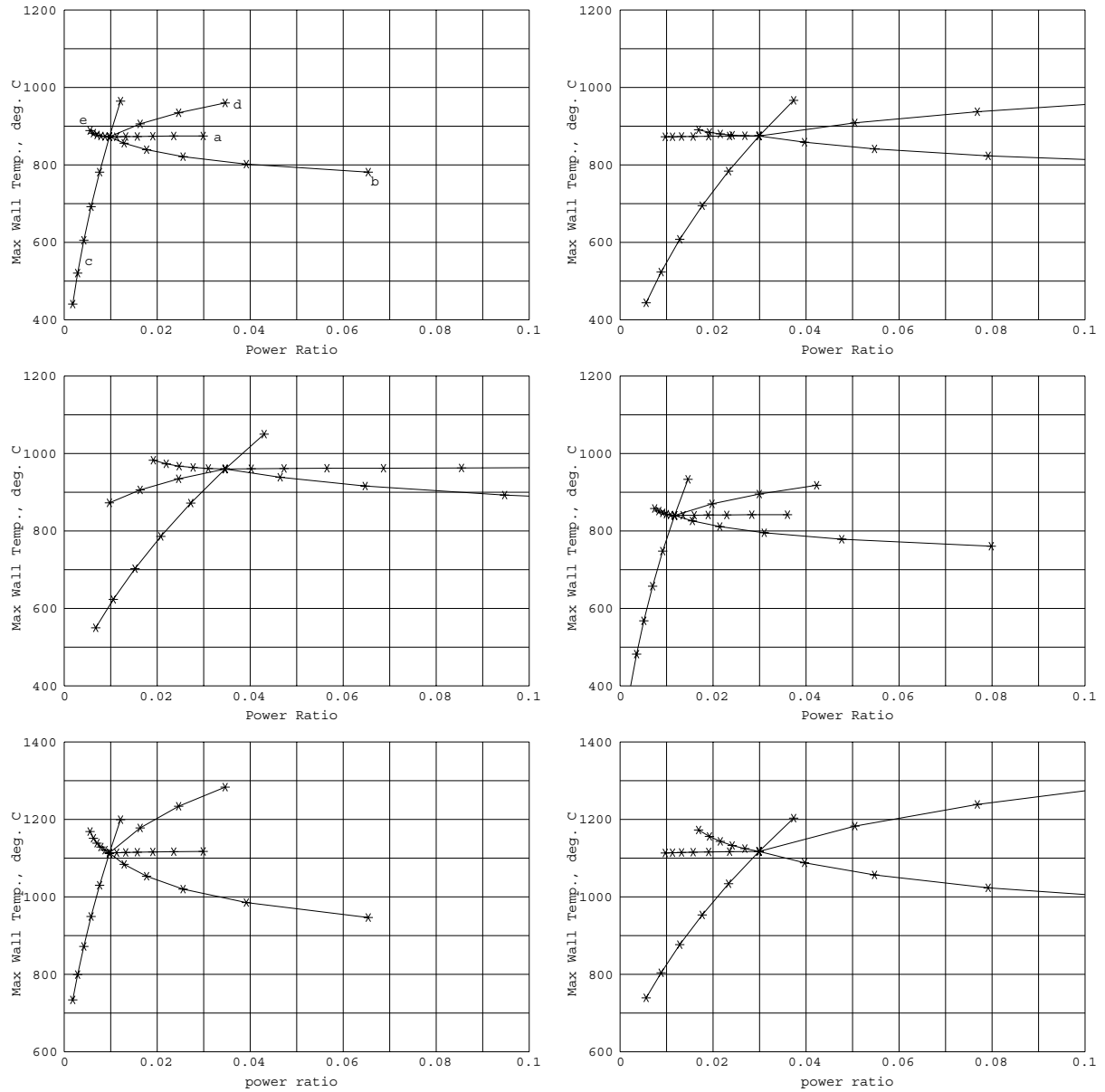
Figure 12: Variation of parameter centre points for the porous medium concept

Curves a, b, c, d, e refer to parameter ranges defined in paragraph iv on page 18 with the following changes of the reference point (PM layer thickness 3 mm, system pressure 14 MPa, uniform heat load 3 MW/m^2):
top left: no changes
top right: system pressure 8 MPa instead of 14 MPa
centre left: uniform heat load 6 MW/m^2 instead of 3 MW/m^2
centre right: PM layer 2.5 mm instead of 3 mm
bottom left: non-uniform heat load with 3 MW/m^2 average, 6 MW/m^2 peak
bottom right: non-uniform heat load with 3 MW/m^2 average, 6 MW/m^2 peak, system pressure 8 MPa instead of 14 MPa
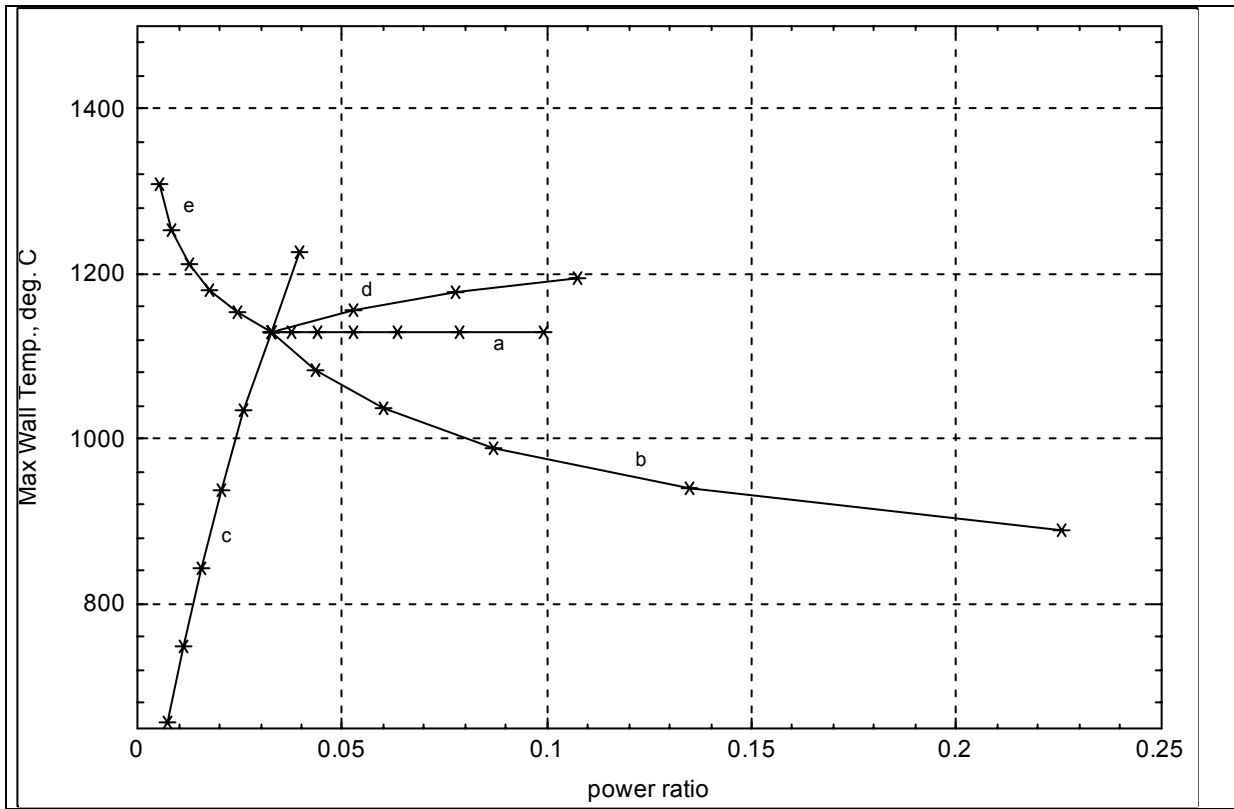
Figure 13: Thermal-hydraulic performance of the multi-channel concept

(Curves a, b, c, d, e refer to parameter ranges defined in paragraph iv on page 18)
top: assuming ideal contact of channel wall and flow channel insert
bottom: assuming no contact of channel wall and flow channel insert

Figure 14: Variation of parameter centre points for the multi-channel concept

(Curves a, b, c, d, e refer to parameter ranges defined in paragraph iv on page 18)
top: no changes
middle: assuming no contact of channel wall and flow channel insert
bottom: operating point suggested in [2], assuming ideal contact of channel wall and flow channel insert

Figure 15: Thermal-hydraulic performance of the swirl rod insert concept

Curves a, b, c, d, e refer to parameter ranges defined in paragraph iv on page 18
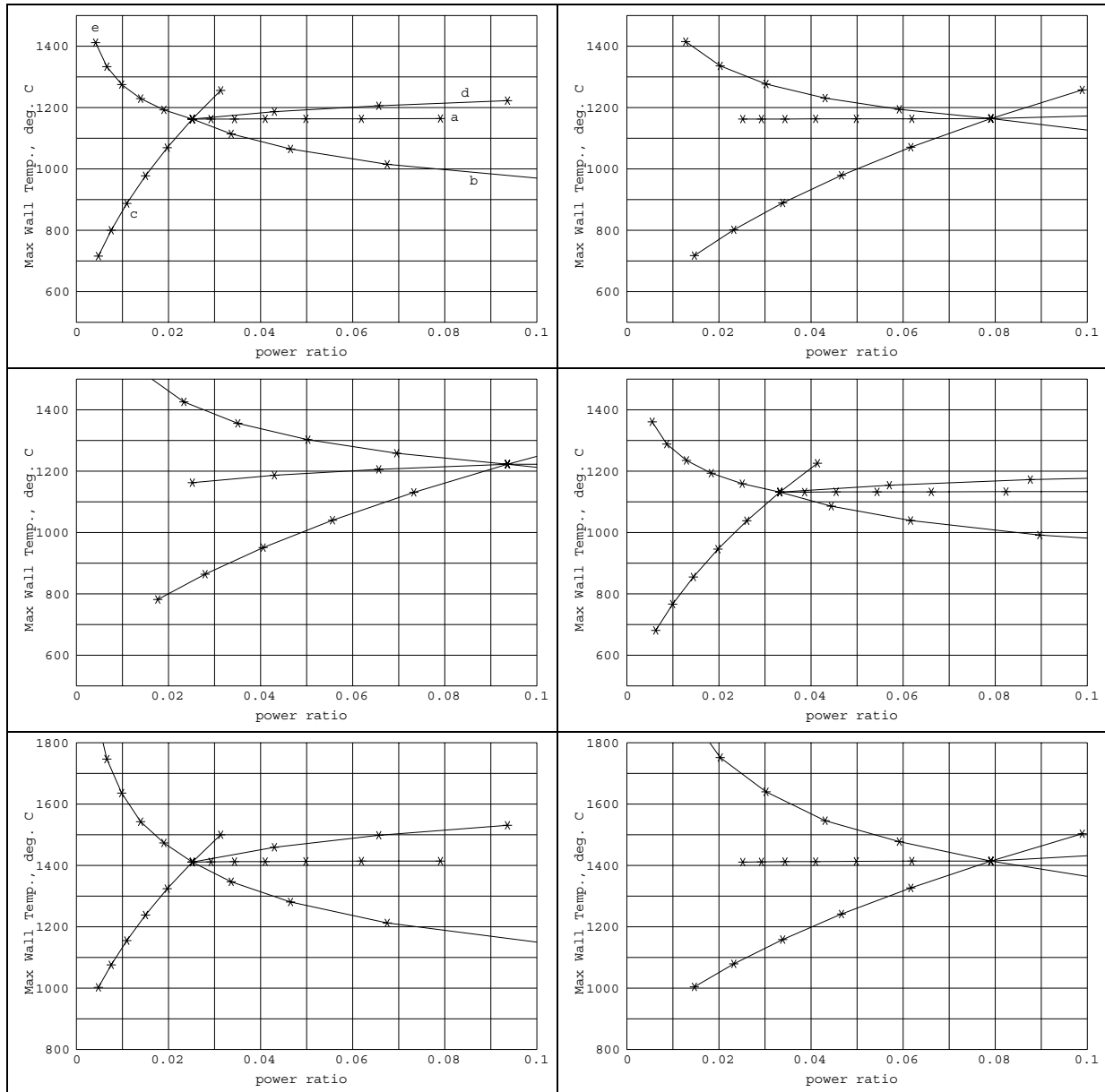
Figure 16: Variation of parameter centre points for the swirl rod insert concept

Curves a, b, c, d, e refer to parameter ranges defined in paragraph iv on page 18 with the following changes of the reference point (channel radial width 2.2mm, system pressure 14 MPa, uniform heat load 3 MW/m^2):
top left: no changes
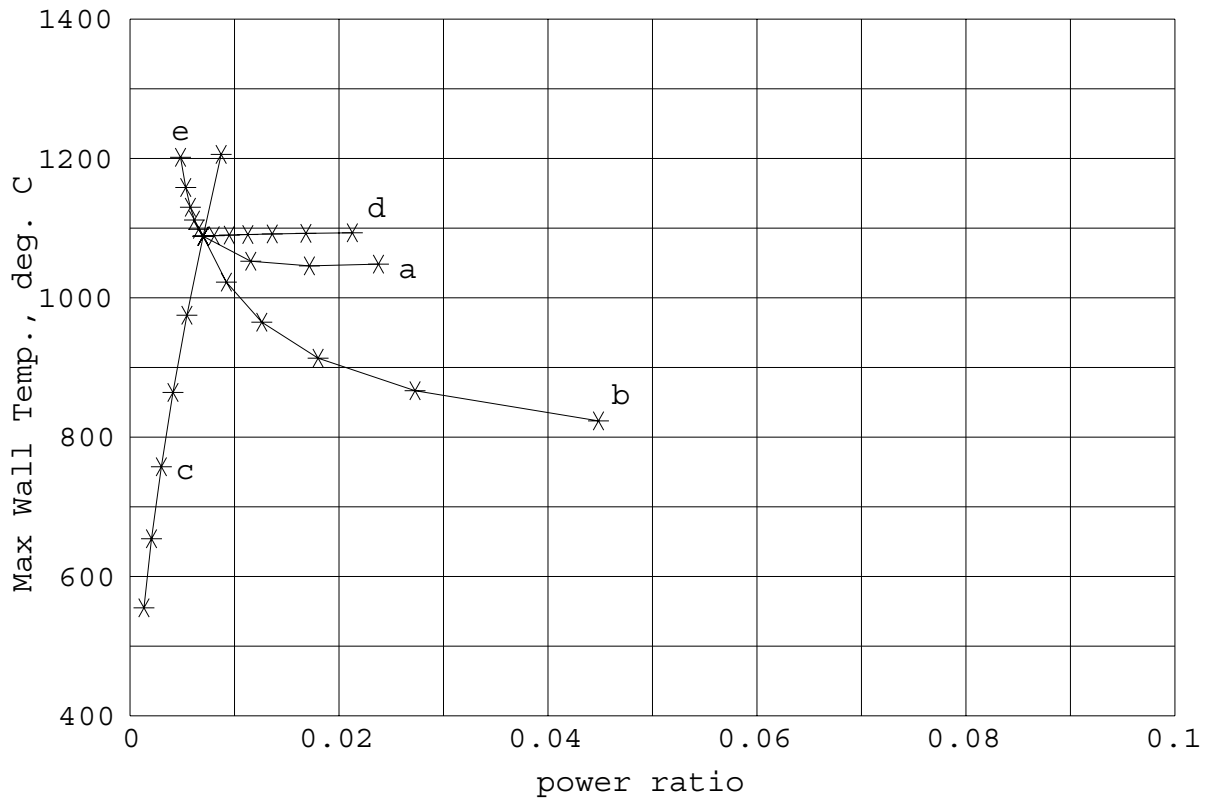top right: system pressure 8 MPa instead of 14 MPa
centre left: uniform heat load 6 MW/m^2 instead of 3 MW/m^2
centre right: channel radial width 2.0 mm instead of 2.2 mm
bottom left: non-uniform heat load with 3 MW/m^2 average, 6 MW/m^2 peak
bottom right: non-uniform heat load with 3 MW/m^2 average, 6 MW/m^2 peak, system pressure 8 MPa instead of 14 MPa
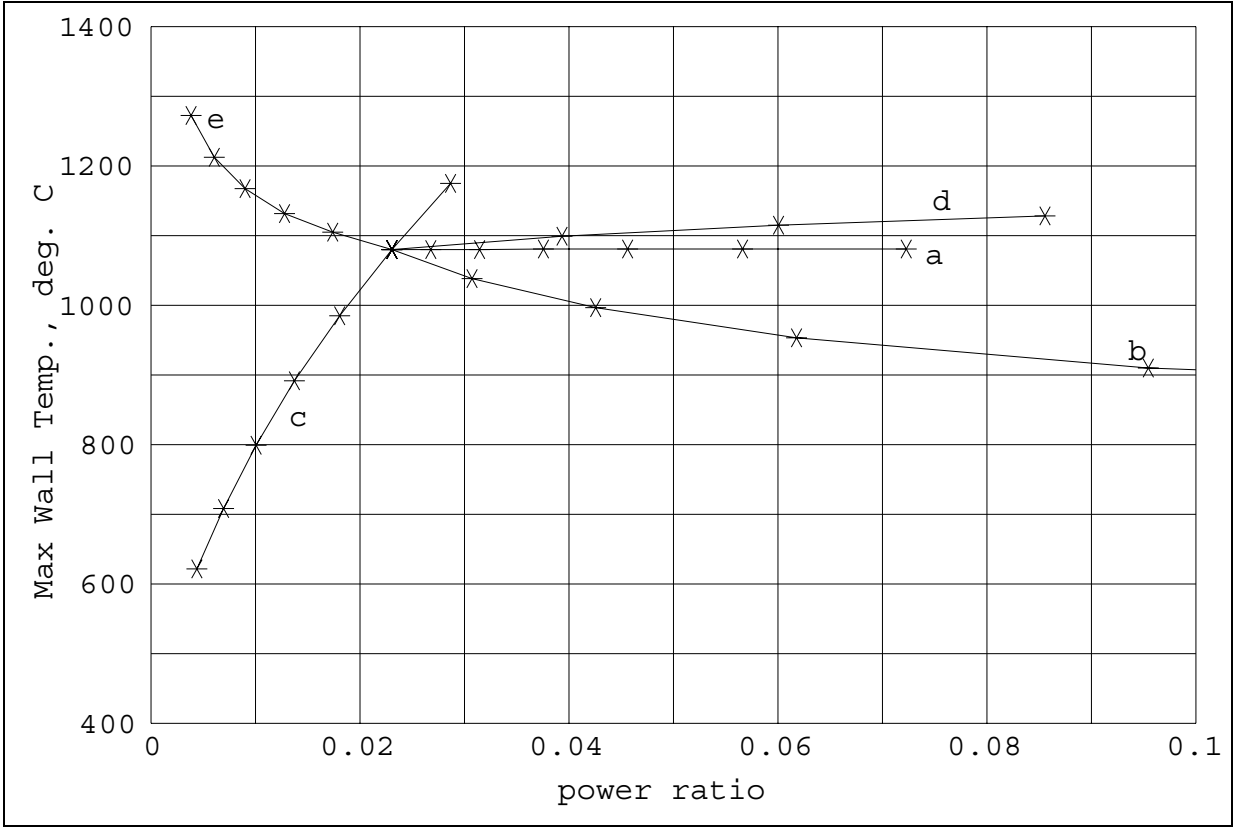
Figure 17: Thermal-hydraulic performance of the eccentric swirl promoter concept

(Curves a, b, c, d, e refer to parameter ranges defined in paragraph iv on page 18)
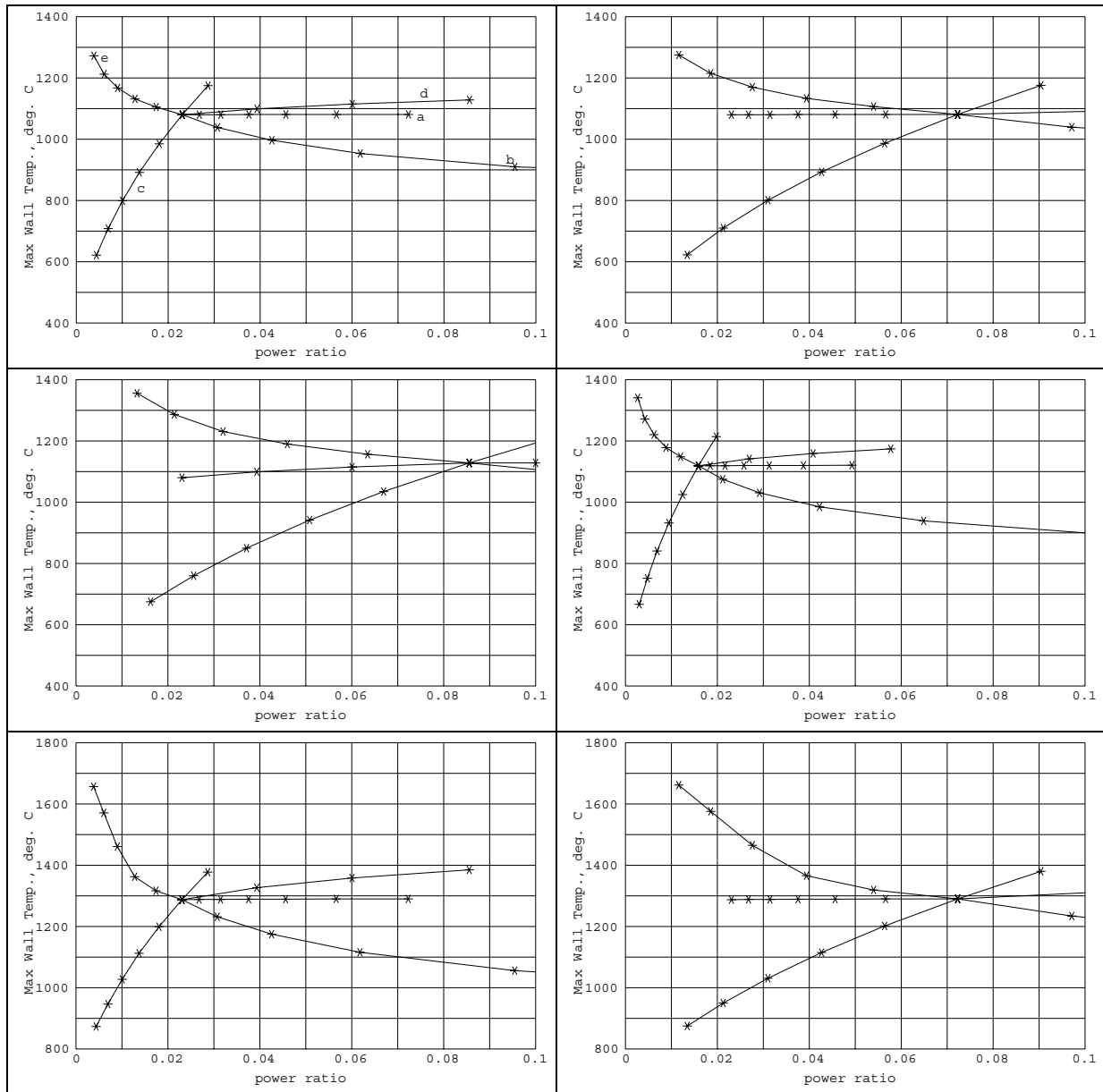
Figure 18: Variation of parameter centre points for the eccentric swirl promoter concept

Curves a, b, c, d, e refer to parameter ranges defined in paragraph iv on page 18 with the following changes of the reference point (eccentricity 0.2mm, system pressure 14 MPa, uniform heat load 3 MW/m^2):
top left: no changes
top right: system pressure 8 MPa instead of 14 MPa
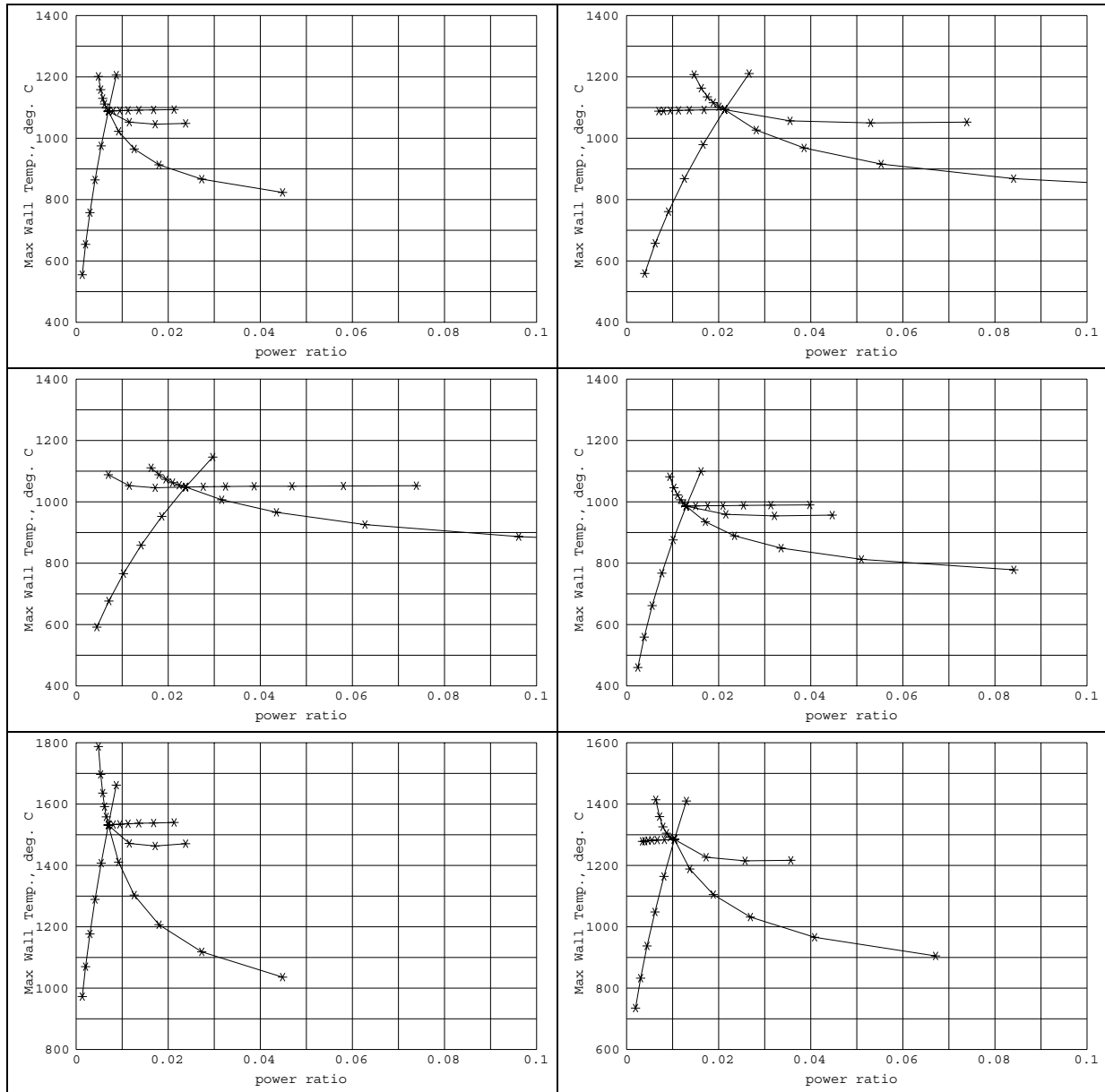centre left: uniform heat load 6 MW/m^2 instead of 3 MW/m^2
centre right: eccentricity 0.15 mm instead of 0.2 mm
bottom left: non-uniform heat load with 3 MW/m^2 average, 6 MW/m^2 peak
bottom right: non-uniform heat load with 3 MW/m^2 average, 6 MW/m^2 peak, system pressure 8 MPa instead of 14 MPa

Figure 19: Thermal-hydraulic performance of the slot concept

(Curves a, b, c, d, e refer to parameter ranges defined in paragraph iv on page 18)

Figure 20: Variation of parameter centre points for the slot concept

Curves a, b, c, d, e refer to parameter ranges defined in paragraph iv on page 18 with the following changes of the reference point (width of slot 0.15 mm, system pressure 14 MPa, uniform heat load 3 MW/m^2):
top left: no changes
top right: system pressure 8 MPa instead of 14 MPa
centre left: uniform heat load 6 MW/m^2 instead of 3 MW/m^2
centre right: width of slot 0.12 mm instead of 0.15 mm
bottom left: non-uniform heat load with 3 MW/m^2 average, 6 MW/m^2 peak
bottom right: non-uniform heat load with 3 MW/m^2 average, 6 MW/m^2 peak, system pressure 8 MPa instead of 14 MPa
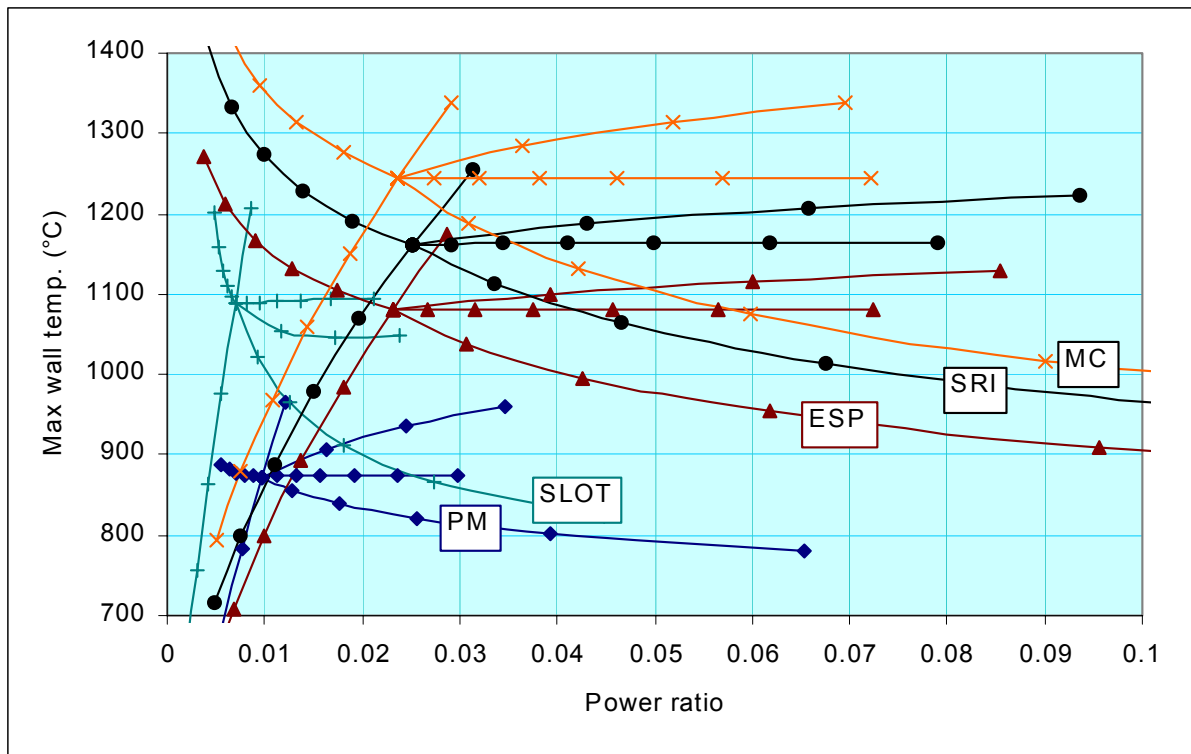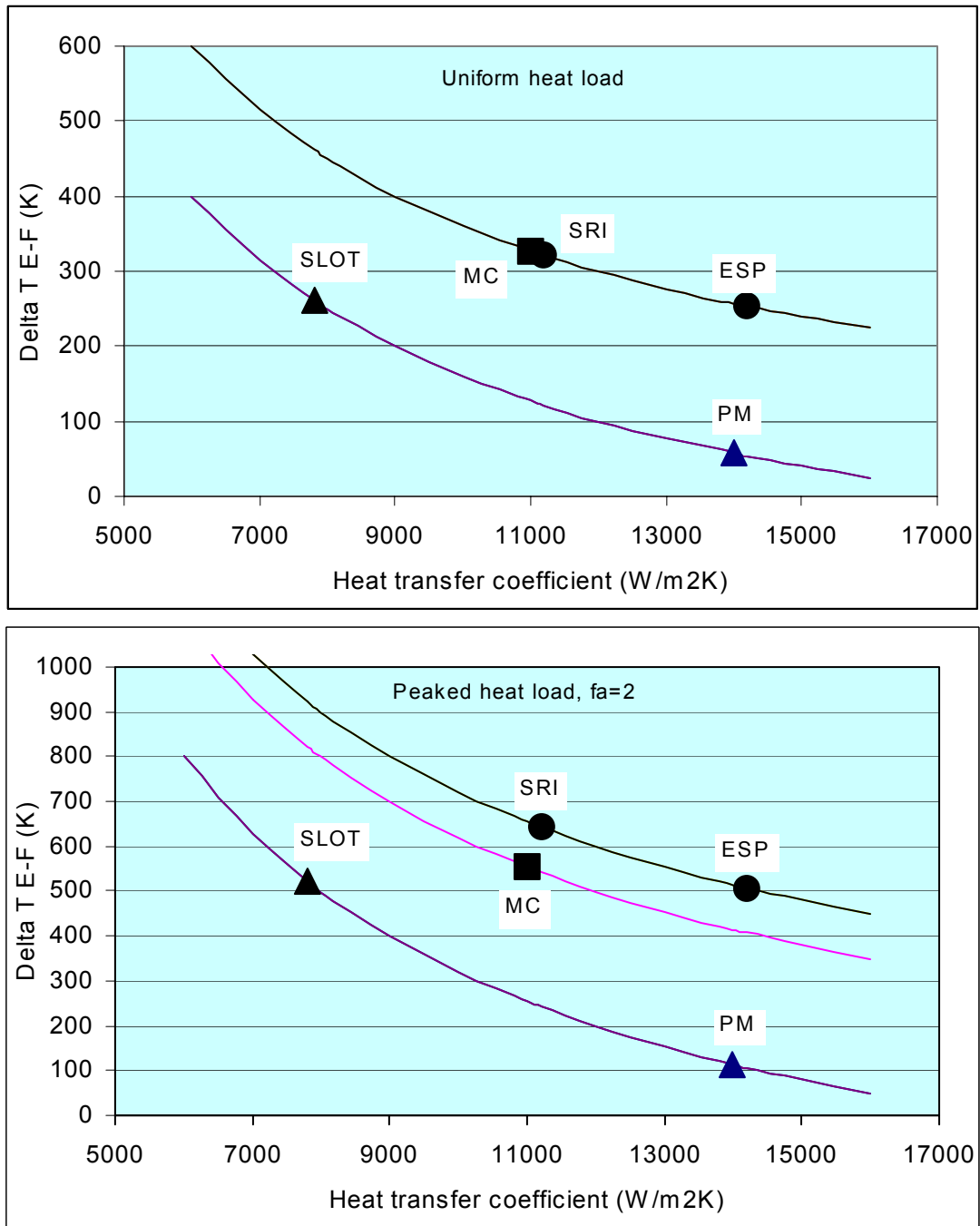
Figure 21: Overlay of thermal-hydraulic performance plots for the concepts studied

Figure 22: Temperature difference between channel front and back as thermal stress indicator

Average heat load: 3 MW/m^2
Heated length: 1 m
System pressure: 14 MPa
Heat transfer coefficients as in according to concept
Coolant temperature rise: 200 K
Axial surface heat flux profile uniform (top) and peaked (bottom)
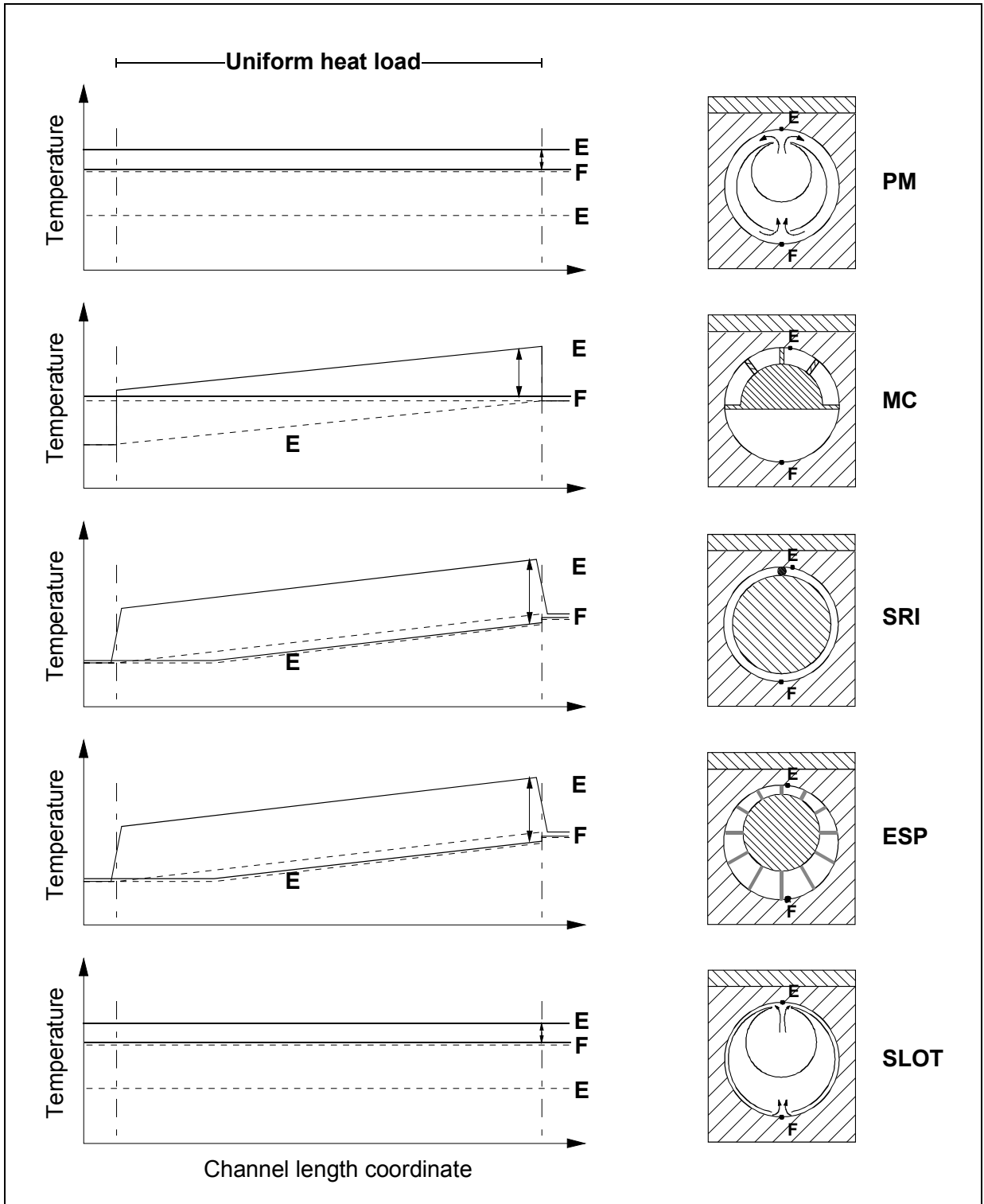
Figure 23: Axial temperature distribution along lines through points E and F (schematic)

Note: Dashed lines show coolant temperature, solid lines show structure temperature for a uniform heat load profile. The largest structural temperature difference between E and F (see the double-arrow lines) is an indicator for the thermal stress that occurs in the channel structure.